CERN-EP-2023-180
24 August 2023

Search for jet quenching effects in high-multiplicity pp collisions at $\sqrt{s} = 13$ TeV via di-jet acoplanarity

ALICE Collaboration*

Abstract

The ALICE Collaboration reports a search for jet quenching effects in high-multiplicity (HM) proton–proton collisions at $\sqrt{s} = 13$ TeV, using the semi-inclusive azimuthal-difference distribution $\Delta\phi$ of charged-particle jets recoiling from a high transverse momentum (high- $p_{T,\text{trig}}$) trigger hadron. Jet quenching may broaden the $\Delta\phi$ distribution measured in HM events compared to that in minimum bias (MB) events. The measurement employs a $p_{T,\text{trig}}$ -differential observable for data-driven suppression of the contribution of multiple partonic interactions, which is the dominant background. While azimuthal broadening is indeed observed in HM compared to MB events, similar broadening for HM events is observed for simulations based on the PYTHIA 8 Monte Carlo generator, which does not incorporate jet quenching. Detailed analysis of these data and simulations show that the azimuthal broadening is due to bias of the HM selection towards events with multiple jets in the final state. The identification of this bias has implications for all jet quenching searches where selection is made on the event activity.

arXiv:2309.03788v2 [hep-ex] 7 Jun 2024

1 Introduction

Strongly-interacting matter at extreme temperature and density forms quark–gluon plasma (QGP), a state in which the dominant degrees of freedom are sub-hadronic [1, 2]. The QGP filled the early universe, and it is generated today in the collision of heavy atomic nuclei at the Relativistic Heavy Ion Collider (RHIC) at Brookhaven National Laboratory and at the Large Hadron Collider (LHC) at CERN. Measurements at these facilities, and their comparison with theoretical calculations based on viscous relativistic hydrodynamics, show that the QGP exhibits complex collective behavior, flowing with very low specific shear viscosity [3].

A key question in the experimental study of the QGP is the limit of its formation in terms of the size of the colliding nuclei. To explore this question, measurements have been carried out for “small collision systems”, in which one of the projectiles is a proton or light nucleus and the other a heavy nucleus, additionally with selection of high event activity (EA) such as produced particle multiplicity or forward neutron production (see e.g. Ref. [4]). Final-state hadronic distributions in small systems exhibit experimental signatures which are associated with production of the QGP in heavy-ion collisions [5], including collective flow [6–9] and enhancement in the production of strange hadrons [10].

Jets are the hadronic remnants of hard (high momentum transfer Q^2) interactions of quarks and gluons from the hadronic projectiles. Measurements of jet production and jet structure in elementary collisions are well described by theoretical calculations based on perturbative QCD (pQCD) [11–13]. In heavy-ion collisions, jets interact with the QGP, resulting in modifications of jet production rates, structure, and angular distributions, which provide incisive probes of the QGP (“jet quenching”) [14, 15].

Jet quenching is a necessary consequence of QGP formation in small systems, though its effects are expected to be small [16–22]. A common signature of jet quenching is the suppression of inclusive hadron or jet yield measured in heavy-ion collisions compared to that expected by scaling the corresponding yield measured in minimum-bias (MB) pp collisions, using a Glauber modeling of the collision geometry [14, 15, 23]. Inclusive jet yield suppression has been reported using this approach in EA-selected d–Au collisions at RHIC (EA based on forward multiplicity) [24] and in p–Pb collisions at the LHC (EA based on forward transverse energy E_T) [25]. However, Glauber modeling using these EA metrics in small systems is subject to significant non-geometric bias [4, 22, 26–32]. An alternative choice for the EA metric, based on zero-degree neutron measurements (nZDC), is found to be less biased, though the scaling still has model-dependent assumptions and uncertainties [4]. Such biases and uncertainties limit the sensitivity of the measurement of jet quenching effects in small systems using Glauber-scaled inclusive yield observables. At present there is no significant evidence, beyond experimental uncertainties, of jet quenching in small systems using this approach [33–35].

The PHENIX Collaboration has recently searched for jet quenching in d–Au collisions at a center-of-mass energy per nucleon–nucleon collision $\sqrt{s_{NN}} = 200$ GeV by the measurement of both π^0 and direct photon (γ_{dir}) inclusive yields in collisions selected by EA [32]. Jet quenching is studied using the γ_{dir} inclusive yield to estimate empirically the rate of hard processes, which does not depend upon Glauber scaling. Strong suppression in the ratio of π^0 and γ_{dir} inclusive yields is observed for high-EA relative to MB collisions, though with absolute value that is consistent with unity within the normalization uncertainty.

An alternative approach has been proposed to search for medium-induced inclusive yield suppression in small systems utilizing MB collisions of light nuclei [19, 20], which likewise does not require Glauber modeling for the yield scaling. However, this approach cannot be applied to EA-selected event populations in small collision systems, where the strongest signals characteristic of collective flow have been observed [6–10].

The comprehensive search for jet quenching effects in small collision systems therefore also requires

approaches based on coincidence observables, which are self-normalized and likewise do not require a Glauber model calculation of nuclear geometry for an EA-selected population. The measurement of jets recoiling from a high- p_T hadron trigger in p–Pb collisions at $\sqrt{s_{NN}} = 5.02$ TeV has set a limit of 0.4 GeV/ c (90% confidence) for medium-induced energy transport to angles greater than 0.4 radians relative to the jet axis, for high-EA collisions selected with criteria based both on forward multiplicity and on nZDC [36]. Measurement of the distribution of hadrons recoiling from a high- p_T jet trigger in EA-selected (nZDC) p–Pb collisions at $\sqrt{s_{NN}} = 5.02$ TeV likewise finds no significant jet quenching signal within uncertainties [37]. The measurement of azimuthal anisotropy of high- p_T hadrons finds small but non-zero second Fourier coefficient v_2 for events selected by EA based on forward E_T [38], though such effects cannot be attributed solely to jet quenching.

It therefore remains an open question whether the collective effects observed in small systems are indeed due to QGP formation, or whether they arise from other phenomena [22, 39–41]. New searches for jet quenching effects in small systems are required to resolve this issue.

In this article we present a novel search for jet quenching effects in EA-selected high-multiplicity (HM) pp collisions at $\sqrt{s} = 13$ TeV. Since “collision geometry” is ill-defined for EA-selected pp collisions, inclusive observables are not appropriate for such a search. Rather, we utilize the semi-inclusive hadron+jet acoplanarity observable [36, 42–45], i.e. the distribution of the azimuthal angle $\Delta\phi$ between a high- p_T hadron trigger and correlated recoil jets, comparing $\Delta\phi$ measurements in HM-selected and MB populations. Jets are reconstructed from charged particles using the anti- k_T algorithm [46] with resolution parameter $R = 0.4$. Jet quenching in the QGP is expected to broaden the $\Delta\phi$ distribution relative to that in vacuum, due to in-medium multiple scattering [47–52]. Indeed, significant in-medium acoplanarity broadening has been observed in central Pb–Pb collisions for large- R recoil jets at low p_T , though the physical mechanisms underlying this broaden remain an open question [44, 45]. However, at present there is no theoretical guidance for the magnitude of the jet transport parameter \hat{q} [14] or alternative characterizations of jet quenching in EA-selected pp collisions, and this is therefore entirely an experiment-driven search.

The analysis is based on the Δ_{recoil} observable developed for semi-inclusive coincidence measurements of jets recoiling from a high- p_T hadron trigger [42]. Precise suppression of jet yield uncorrelated with the trigger particle (uncorrelated background yield) is crucial in this analysis, since the uncorrelated yield of jets generated by multiple partonic interactions (MPI) from independent high- Q^2 processes can mimic azimuthal broadening arising from jet quenching. The Δ_{recoil} observable provides data-driven suppression of uncorrelated background yield through the difference of trigger hadron-normalised recoil jet distributions in two exclusive trigger p_T intervals (Sec. 5). Selection of the HM population utilizes a large data sample recorded by ALICE with an online HM trigger during the 2016–2018 LHC pp runs at $\sqrt{s} = 13$ TeV. The $\Delta\phi$ distributions from the HM-selected and MB event populations are compared, revealing a striking acoplanarity broadening in HM-selected events. However, similar broadening is also observed in PYTHIA-based simulations. The physical origin of the broadening is elucidated through a detailed study of the rapidity dependence of jet production and the number of recoil jets in HM-selected and MB-selected events.

The paper is organized as follows: Sec. 2 presents the data set and offline analysis; Sec. 3 presents characterization of event activity using forward multiplicity; Sec. 4 presents jet reconstruction; Sec. 5 presents the coincidence observable Δ_{recoil} ; Sec. 6 presents data corrections; Sec. 7 presents systematic uncertainties; and Sec. 8 presents the physics results and their interpretation.

2 Data set and offline analysis

The ALICE detector and its performance are described in Refs. [53, 54]. Data for this analysis were recorded during the 2016, 2017, and 2018 LHC runs with pp collisions at $\sqrt{s} = 13$ TeV. Events were

selected online using signals in the V0 detectors [55], which are plastic scintillator arrays covering the pseudorapidity ranges $2.8 < \eta < 5.1$ (V0A) and $-3.7 < \eta < -1.7$ (V0C). The V0 signal is proportional to the total number of charged particles (multiplicity) in the detector acceptance. Two different V0 trigger configurations were employed, called minimum bias (labelled “MB”) and high multiplicity (“HM”). The MB trigger required the in-time coincidence of V0A and V0C signals, while the HM trigger required the sum of V0A and V0C signal amplitudes (denoted as V0M) to be at least five times larger than the mean signal amplitude in MB events (denoted as $\langle V0M \rangle$). The HM trigger selected 0.1% of MB events with the largest value of V0M.

The EA is characterized offline by the scaled V0 signal, $V0M/\langle V0M \rangle = (V0A + V0C)/\langle V0A + V0C \rangle$, which is insensitive to changes in V0 gain in the different data-taking periods due to scintillator aging. It also provides ordering of events in terms of EA without the need for precise calculation of the absolute V0 signal in model calculations, for a well-defined comparison of such models with data. The value of $\langle V0M \rangle$ is calculated separately for each data-taking run lasting a few hours, as a function of the collision vertex position along the beam axis. The HM selection is further constrained in the offline analysis to the range $5 < V0M/\langle V0M \rangle < 9$. The lower bound of 5 is determined by the online HM trigger threshold, while the upper bound of 9 is determined by the range over which the $V0M/\langle V0M \rangle$ distributions for the three different measurement periods are consistent; higher values may be affected by residual, uncorrected pileup effects.

In the offline analysis, jets are measured at midrapidity using charged particles reconstructed with the ALICE central barrel detectors, covering the range $|\eta| < 0.9$. Track reconstruction is based on space points measured by the Inner Tracking System (ITS) and Time Projection Chamber (TPC) [54]. Primary event vertices are reconstructed offline based on global tracks, which are required to have space points in the Silicon Pixel Detector (SPD) forming the two innermost layers of the ITS. Accepted events are required to have the primary vertex within $|z_{\text{vtx}}| < 10$ cm, where z_{vtx} is the location of the vertex along the beam axis relative to the nominal center of the ALICE detector.

For MB-triggered events, the pileup rate due to multiple hadronic pp collisions in the same LHC bunch crossing is less than 3.5%. The pile-up contribution is suppressed offline by rejecting events with multiple reconstructed event vertices. Monte Carlo studies estimate that the residual pileup contribution following this cut is negligible for the MB populations and about 1% for the HM population. As discussed in Sec. 5, the observable Δ_{recoil} used in the analysis provides data-driven suppression of uncorrelated background yield, which also includes residual pileup events that are not rejected by the multiple-vertex algorithm. After event selection, the data sets have an integrated luminosity of 32 nb^{-1} for the MB trigger and 10 pb^{-1} for the HM trigger.

During the data taking, the ITS had non-uniform efficiency, and the analysis therefore utilizes hybrid tracks [13, 56] to achieve azimuthally uniform tracking response. Hybrid tracks consist of good quality global tracks with at least one hit in the SPD, and complementary tracks without SPD signals. To ensure good momentum resolution, the momentum of these complementary tracks is determined using the primary vertex as a constraint. Reconstructed tracks with $|\eta| < 0.9$ and $p_{\text{T}} > 0.15 \text{ GeV}/c$ are accepted for the analysis. Hybrid track reconstruction efficiency is 0.85 at $p_{\text{T}} = 1 \text{ GeV}/c$, 0.82 at $p_{\text{T}} = 10 \text{ GeV}/c$, and 0.74 at $p_{\text{T}} = 50 \text{ GeV}/c$. Tracking efficiencies for MB and HM events are similar. Primary-track momentum resolution is 0.7% at $p_{\text{T}} = 1 \text{ GeV}/c$, 1.3% at $p_{\text{T}} = 10 \text{ GeV}/c$, and 3.7% at $p_{\text{T}} = 50 \text{ GeV}/c$.

Simulations are utilized for data corrections and for comparison to theoretical calculations. The simulations are based on the PYTHIA 8 event generator [57] with Monash tune [58], and a detailed GEANT3 model [59] of the ALICE detector response, which includes production of secondary particles and realistic hit digitization. Events generated by PYTHIA 8 without detector effects are denoted “particle-level,” and such events passed through GEANT3 are denoted “detector-level.”

For particle-level events, the V0A and V0C responses are determined by counting the number of charged

particles in their acceptance. The coincidence requirement of the online trigger is modeled by requiring particle-level events to have particles in both V0A and V0C, while detector-level events are required to have GEANT-generated hits in both V0A and V0C. The MB events are used to calculate the V0M distributions at both detector and particle level.

3 V0M/ \langle V0M \rangle distributions

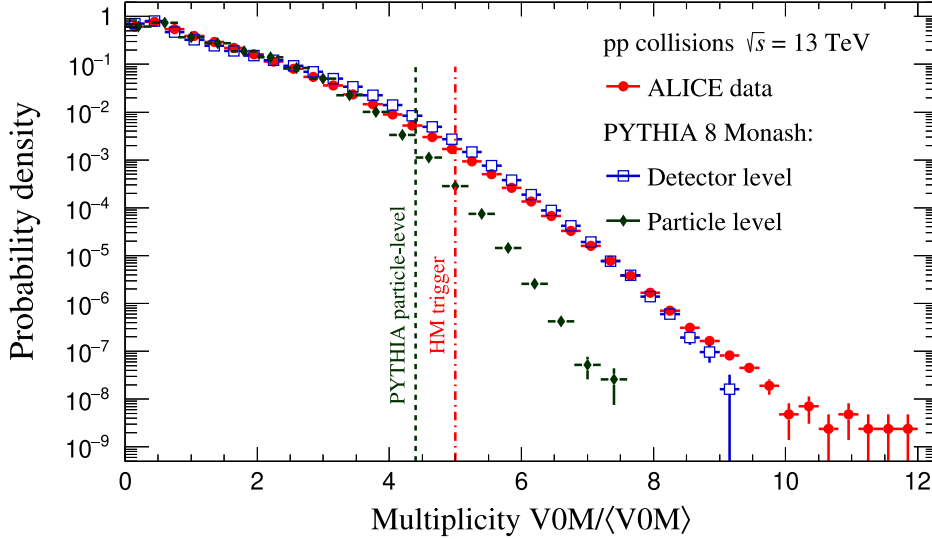


Figure 1: Probability distribution of $V0M/\langle V0M \rangle$ in MB pp collisions measured at $\sqrt{s} = 13$ TeV, and in simulated MB pp events generated by PYTHIA 8 at the particle and detector level. The vertical dashed lines indicate the lower bound for HM selection for data and particle-level simulations.

Figure 1 shows the $V0M/\langle V0M \rangle$ probability distribution for MB pp collisions at $\sqrt{s} = 13$ TeV. The lower limit for HM event selection, $V0M/\langle V0M \rangle = 5$, is indicated by the red dashed-dotted line. The figure also shows the $V0M/\langle V0M \rangle$ probability distribution at the particle and detector level for PYTHIA 8-generated events for MB pp collisions at $\sqrt{s} = 13$ TeV. These distributions differ because of a large contribution at forward angles of secondary particles generated in detector material [60]. The particle-level distribution falls more rapidly than that observed in data in the range $V0M/\langle V0M \rangle > 4$. However, the detector-level distribution qualitatively reproduces that observed in data, with probability densities which lie within a factor ~ 2 of each other over a range of nine orders of magnitude in $V0M/\langle V0M \rangle$.

In order to compare PYTHIA 8 particle-level HM-selected distributions to data, we assume that the secondary particle yield due to interactions in detector material is on average proportional to the primary multiplicity in the V0 acceptance. The HM selection for the particle-level distribution is therefore chosen to select the same fraction of the MB cross section (0.1%) as the HM selection $V0M/\langle V0M \rangle > 5.0$ used for data. This selection corresponds to particle-level $V0M/\langle V0M \rangle > 4.4$, as indicated by the dark dashed line in Fig. 1.

We note, however, that such selections of the same cross section fraction at the particle and detector level only select the same fraction of the distributions. They cannot select the same population event-by-event, due to significant fluctuations in the correlation between particle- and detector-level events. For the detector model used in this study, about 35% of events passing the HM selection at the detector level also do so at the particle level. This is a generic issue, with similar features expected for any event selection in small systems based on forward EA.

4 Jet reconstruction

Jet measurements in this coincidence analysis are corrected for two distinct background effects: uncorrelated jet yield, which is corrected using the Δ_{recoil} observable discussed in Sect. 5; and p_{T} -smearing of correlated jets due to overlap with uncorrelated background components, as detailed in this section. These corrections are carried out in distinct analysis steps.

Several types of reconstructed jets are consequently used in the analysis, which are distinguished using the notation defined in Refs. [36, 42]. For data, $p_{\text{T,jet}}^{\text{raw,ch}}$ refers to the raw output of the jet reconstruction algorithm; $p_{\text{T,jet}}^{\text{reco,ch}}$ refers to $p_{\text{T,jet}}^{\text{raw,ch}}$ after subtraction of the event-wise estimate of the background contribution to $p_{\text{T,jet}}$, $\rho \times A_{\text{jet}}$, which is the product of median jet p_{T} density in the event and the jet area (Eq. 1); and $p_{\text{T,jet}}^{\text{ch}}$ refers to the fully corrected jet transverse momentum. For simulations, $p_{\text{T,jet}}^{\text{part}}$ refers to charged-particle jets at the particle level, and $p_{\text{T,jet}}^{\text{det}}$ charged-particle jets at the detector level; both quantities are corrected by $\rho \times A_{\text{jet}}$ using the following procedure.

Jets are reconstructed from accepted charged-particle tracks. Particles are assumed to be massless and their four-momenta are combined with the boost-invariant p_{T} recombination scheme [61]. Jet reconstruction is carried out twice for each event. The first reconstruction pass uses the k_{T} algorithm [61] with $R = 0.4$ and accepts jets with $|\eta_{\text{jet}}| < 0.9 - R$. The first-pass jet population is used to determine ρ , the event-wise estimate of the background energy density [62],

$$\rho = \text{median} \left\{ \frac{p_{\text{T,jet}}^{\text{raw,ch},i}}{A_{\text{jet}}^i} \right\}, \quad (1)$$

where $p_{\text{T,jet}}^{\text{raw,ch},i}$ and A_{jet}^i are the raw jet p_{T} and the area [63] of the i^{th} jet in the event. Jet area is calculated using the ghost area method of FastJet, with a ghost area of 0.005 [63]. The two hardest jets in the event are excluded from the median calculation. The most probable value of ρ is zero in both the MB and HM populations, while the mean value of ρ is 0.09 GeV/ c for MB and 1.24 GeV/ c for HM-selected events. For events containing a charged track in $|\eta| < 0.9$ with $20 < p_{\text{T}} < 30$ GeV/ c , the mean value of ρ is 0.39 GeV/ c for MB and 1.62 GeV/ c for HM events.

The second reconstruction pass uses the anti- k_{T} algorithm [61] with $R = 0.4$. The acceptance for the second pass is likewise $|\eta_{\text{jet}}| < 0.9 - R$ over the full azimuth.

The jet p_{T} obtained from the second pass is then adjusted for the median background p_{T} density ρ according to [62]

$$p_{\text{T,jet}}^{\text{reco,ch}} = p_{\text{T,jet}}^{\text{raw,ch}} - \rho \times A_{\text{jet}}. \quad (2)$$

The jet p_{T} scale and jet p_{T} resolution are the same as in Ref. [64].

5 Observables and raw data

The analysis utilizes a differential observable based on the semi-inclusive distribution of charged-particle jets recoiling from a high- p_{T} trigger (“h+jet”) [42] (see also [36, 43]). The key components of this approach are summarized in this section.

The goal of the analysis is the search for broadening of the $\Delta\phi$ distribution in HM-selected events due to medium-induced jet scattering, by comparison to the MB population. A significant source of uncorrelated background yield to this process arises from MPIs, in which multiple uncorrelated high- Q^2 partonic interactions occur in the same pp collision, with one such interaction generating a trigger hadron and an-

other generating a recoil jet in the acceptance. The $\Delta\phi$ distribution of such MPI pairs is by definition uniform on average, thereby limiting the measurement sensitivity to broadening of the $\Delta\phi$ distribution from medium-induced scattering of correlated recoil jets.

Precise background yield correction must be carried out in a fully data-driven way, without model dependence. We therefore employ the Δ_{recoil} observable [42], which is the difference between semi-inclusive recoil jet distributions for two ranges of $p_{T,\text{trig}}$, both normalized to the number of trigger hadrons,

$$\Delta_{\text{recoil}}(p_T, \Delta\phi) = \frac{1}{N_{\text{trig}}} \frac{d^2 N_{\text{jet}}}{dp_{T,\text{jet}}^{\text{ch}} d\Delta\phi} \Bigg|_{p_{T,\text{trig}} \in \text{TT}_{\text{Sig}}} - c_{\text{Ref}} \times \frac{1}{N_{\text{trig}}} \frac{d^2 N_{\text{jet}}}{dp_{T,\text{jet}}^{\text{ch}} d\Delta\phi} \Bigg|_{p_{T,\text{trig}} \in \text{TT}_{\text{Ref}}}, \quad (3)$$

where TT denotes ‘‘trigger track.’’ In this analysis, $\text{TT}_{\text{Sig}} = \text{TT}\{20, 30\}$ specifies the range $20 < p_{T,\text{trig}} < 30$ GeV/ c for the Signal trigger distribution, and $\text{TT}_{\text{Ref}} = \text{TT}\{6, 7\}$ specifies the range $6 < p_{T,\text{trig}} < 7$ GeV/ c for the Reference trigger distribution. These intervals were chosen to optimize the opposing requirements of obtaining high statistical precision and limiting the kinematic range for more precise comparison of the same observables with different EA selections. The number of trigger hadrons measured in each TT class is denoted N_{trig} . The azimuthal difference $\Delta\phi$ between TT and recoil jet is defined to have the range $[0, \pi]$ radians.

The Δ_{recoil} distribution is a two-dimensional function of $p_{T,\text{jet}}$ and $\Delta\phi$ [36, 42]. We define its one-dimensional projections, $\Delta_{\text{recoil}}(p_{T,\text{jet}})$ and $\Delta_{\text{recoil}}(\Delta\phi)$, onto the $p_{T,\text{jet}}^{\text{reco, ch}}$ and $\Delta\phi$ axes respectively, for restricted ranges in the other kinematic variable. These projections are shown in Figs. 2 and 3 both prior to and after corrections, as indicated by the functional argument (e.g. $\Delta_{\text{recoil}}(p_{T,\text{jet}}^{\text{reco, ch}})$ or $\Delta_{\text{recoil}}(p_{T,\text{jet}}^{\text{ch}})$).

The scaling factor c_{Ref} , which is applied to the Reference distribution (second term in Eq. 3), accounts for the different phase space available to observe uncorrelated yield in the Signal and Reference distributions [42, 43]. In this analysis, the value of c_{Ref} is determined from the ratio of trigger-normalized Signal and Reference recoil jet yields in the bin $0 < p_{T,\text{jet}}^{\text{reco, ch}} < 1$ GeV/ c , which is expected to be dominated by uncorrelated background yield. This gives values $c_{\text{Ref}} = 0.95 \pm 0.03$ (syst.) in MB events and $c_{\text{Ref}} = 0.94 \pm 0.03$ (syst.) in HM events.

Since the uncorrelated yield is by definition independent of TT, it therefore contributes with equal magnitude to the two terms in Eq. 3 and is therefore removed by the subtraction. While Δ_{recoil} is a differential observable and not an absolutely normalized yield, its two terms are nevertheless calculable perturbatively [65]. Measurements of Δ_{recoil} in minimum-bias pp collisions are well described by PYTHIA 8 [36, 42].

In the analysis of both MB and HM-selected events, the dataset is divided into two statistically independent subsets, with the Signal distribution determined using 95% of all events, and the Reference distribution determined using the remaining 5%. These fractions were chosen to provide an equal number of trigger hadrons in the two TT classes, in order to optimize the statistical precision of Δ_{recoil} . The statistical error due to the N_{trig} normalization is negligible.

If two hadrons in an event satisfy the TT condition, one is chosen at random. This selection ensures that the p_T -differential TT distribution has the same shape as the inclusive charged-hadron yield, which is an essential requirement for a semi-inclusive measurement [42].

Figure 2 shows selected $\Delta_{\text{recoil}}(p_{T,\text{jet}}^{\text{reco, ch}})$ and $\Delta_{\text{recoil}}(\Delta\phi)$ distributions, together with their corresponding Signal and Reference distributions. The Signal and Reference distributions have similar magnitude only in the region $p_{T,\text{jet}}^{\text{reco, ch}} < 20$ GeV/ c , while at larger values of $p_{T,\text{jet}}^{\text{reco, ch}}$ the Reference distribution falls below the Signal distribution and Δ_{recoil} is similar in magnitude to the Signal distribution.

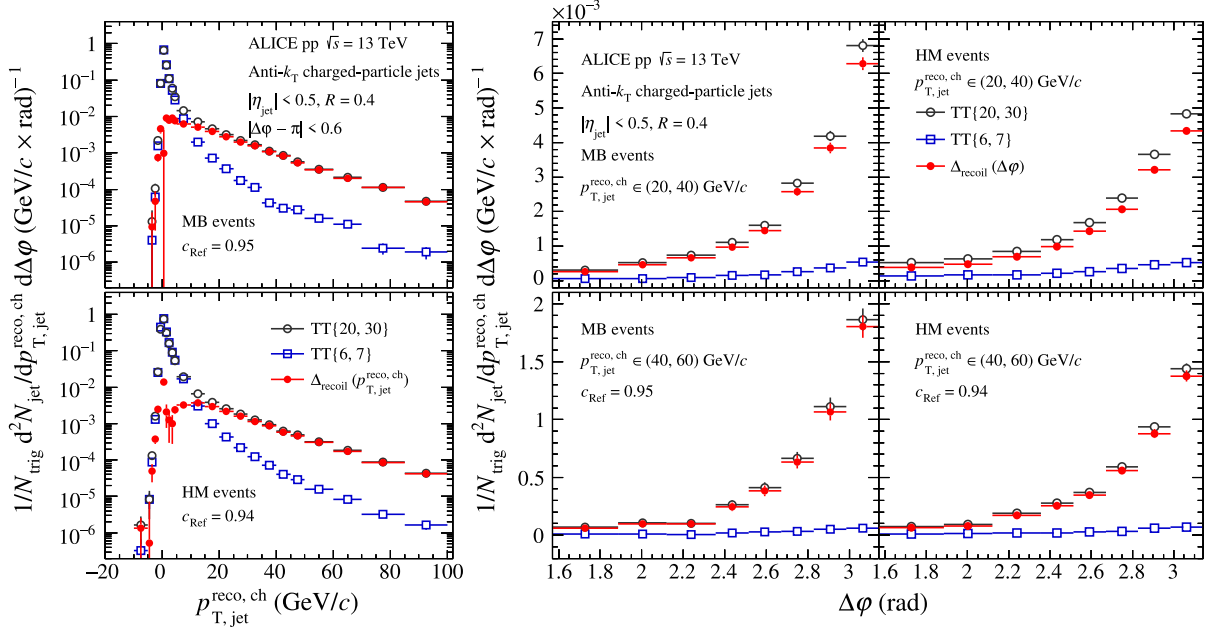


Figure 2: The Signal (TT{20,30}) and Reference (TT{6,7}) trigger-normalized recoil jet distributions and the corresponding Δ_{recoil} distribution for MB and HM pp collisions at $\sqrt{s} = 13$ TeV. Left panels: projection onto $p_{T,\text{jet}}^{\text{reco, ch}}$ for $|\Delta\phi - \pi| < 0.6$. Middle and right panels: projection onto $\Delta\phi$ in two $p_{T,\text{jet}}^{\text{reco, ch}}$ intervals.

6 Corrections

Particle-level jets are clustered from all final-state charged particles generated with PYTHIA 8 as described in Sec. 2, except for weak decay daughters [66, 67]. The measured (detector-level) Δ_{recoil} distribution is corrected to the particle level.

Subtraction of the scaled Reference distribution in Eq. 3 accurately removes the uncorrelated jet yield [42]. However, the resulting Δ_{recoil} distribution is still subject to instrumental effects which smear $p_{T,\text{jet}}$ and $\Delta\phi$, whose correction is discussed in this section. These smearing effects are encoded in the four-dimensional response matrix R_{instr} , which maps the true (particle-level) distribution of Δ_{recoil} onto the measured distribution,

$$\Delta_{\text{recoil}}^{\text{Meas}}(\Delta\phi^{\text{det}}, p_{T,\text{jet}}^{\text{det}}) = R_{\text{instr}}(\Delta\phi^{\text{det}}, p_{T,\text{jet}}^{\text{det}}; \Delta\phi^{\text{part}}, p_{T,\text{jet}}^{\text{part}}) \otimes \Delta_{\text{recoil}}^{\text{True}}(\Delta\phi^{\text{part}}, p_{T,\text{jet}}^{\text{part}}). \quad (4)$$

The $p_{T,\text{jet}}$ and angular smearing due to instrumental effects is very similar in the inclusive and recoil jet populations in these simulations. In addition, the inclusive population has a substantially larger sample in the simulated dataset. The matrix R_{instr} is therefore constructed using the inclusive jet population, by matching particle-level and detector-level jets in phase space within $\Delta R = \sqrt{(\Delta\eta)^2 + (\Delta\phi)^2} < 0.3$. The response matrix has p_T bins of width 1 GeV/c, so that the difference in the spectrum shape of the inclusive and recoil jet populations has negligible effect on this procedure.

Track reconstruction efficiency, which is the dominant instrumental effect, is found to be the same for MB and HM events. The MB and HM analyses therefore use the same response matrix, obtained using MB events. Unmatched particle-level jets are tabulated and their rate is applied as an efficiency correction, following the unfolding correction discussed below. Jet matching efficiency for both MB and HM events is 0.98 at $p_{T,\text{jet}}^{\text{ch}} = 10$ GeV/c and consistent with unity at higher $p_{T,\text{jet}}^{\text{ch}}$.

The corrected Δ_{recoil} distribution is calculated by regularized inversion of Eq. 4, using two-dimensional iterative Bayesian unfolding [68] implemented in the RooUnfold package [69]. The input distribution

$\Delta_{\text{recoil}}^{\text{Meas}}$ is specified in the range $10 < p_{\text{T,jet}}^{\text{det}} < 100$ GeV/ c and $\pi/2 < \Delta\phi^{\text{det}} < \pi$ rad. The prior distribution for initiating the unfolding is the Δ_{recoil} particle-level spectrum calculated using PYTHIA 8 simulations. For unfolding the MB dataset, the prior is calculated using MB PYTHIA 8 events, whereas for unfolding the HM dataset the detector-level HM selection is applied to the simulated data, as shown in Fig. 1.

Regularization is optimized by requiring that the unfolded distributions from successive iterations exhibit a mean change of less than 2%, averaged over all p_{T} bins. The optimum number of iterations using this criterion is found to be 5, for both the MB and HM analyses.

While correction of the Δ_{recoil} distribution for instrumental effects is carried out by regularized unfolding using the full instrumental response matrix R_{instr} , insight into the unfolding procedure can also be gained by parametric characterization of the main detector-level effects. Detector-level effects in $p_{\text{T,jet}}$ are characterized by the jet energy scale shift (JES) between particle-level and detector-level, $\langle (p_{\text{T,jet}}^{\text{det}} - p_{\text{T,jet}}^{\text{part}}) / p_{\text{T,jet}}^{\text{part}} \rangle$, while jet energy resolution (JER) is its width, $\sigma(p_{\text{T,jet}}^{\text{det}}) / p_{\text{T,jet}}^{\text{part}}$, where $\sigma(p_{\text{T,jet}}^{\text{det}})$ is RMS of the $p_{\text{T,jet}}^{\text{det}}$ distribution. For $p_{\text{T,jet}}^{\text{part}} = 10, 40, \text{ and } 70$ GeV/ c , JES is $-10\%, -14\%, \text{ and } -18\%$, and JER is $25\%, 22\%, \text{ and } 23\%$, respectively. Other systematic effects which are not encoded in the response matrix, such as the precision of the ALICE central barrel B -field scale ($\sim 10^{-3}$), make negligible contribution to JES and JER.

Azimuthal angular smearing is likewise found to have the same magnitude in MB and HM events. Azimuthal smearing of tracks contributing to TT{20,30} has RMS $\approx 2 \times 10^{-3}$ rad, while azimuthal smearing of the jet axis has RMS $\approx 26 \times 10^{-3}$ rad for $10 < p_{\text{T,jet}}^{\text{ch}} < 15$ GeV/ c and 11×10^{-3} rad for $60 < p_{\text{T,jet}}^{\text{ch}} < 80$ GeV/ c . The corresponding distributions of $\Delta\phi$ have RMS of 34×10^{-3} rad for $10 < p_{\text{T,jet}}^{\text{ch}} < 15$ GeV/ c and 13×10^{-3} rad for $60 < p_{\text{T,jet}}^{\text{ch}} < 80$ GeV/ c .

Subtraction of the reference distribution in the Δ_{recoil} observable corrects the uncorrelated background yield. However, the resulting two-dimensional distribution as a function of $p_{\text{T,jet}}^{\text{ch}}$ and $\Delta\phi$ is still smeared by residual fluctuations of the uncorrelated background component, which causes the underlying event density to deviate locally from ρ . Correction for such fluctuations requires model assumptions (see e.g. Refs. [35, 64]) and is therefore not included in the unfolding; rather, its magnitude is assessed for two common model choices and the variation in unfolded distributions is included in the systematic uncertainty, as discussed in Sec. 7.4.

The unfolding procedure is validated by a closure test in which the input is PYTHIA 8 detector-level events, the full analysis chain, including unfolding, is carried out, and the output is compared to the particle-level PYTHIA 8 spectrum. Good agreement between both distributions is found within statistical uncertainties, thereby confirming the robustness of the applied corrections.

7 Systematic uncertainties

The main sources of systematic uncertainty in the measurement of Δ_{recoil} are related to track reconstruction efficiency; track p_{T} resolution; the unfolding procedure; the determination of the scaling factor c_{Ref} ; and residual background p_{T} -density fluctuations relative to ρ . The systematic uncertainty due to each source is estimated by varying the appropriate parameters and rerunning the full analysis chain.

However, the finite statistical precision of the data imposes a limit on the precision with which the spectrum can be unfolded. This limit is taken into account in the determination of the systematic uncertainties by using the following procedure, which is described in detail in Ref. [36]. For each parameter variation the spectrum is unfolded 10 times, with the central values of the spectrum varied randomly and independently using a Poisson distribution corresponding to the statistical error of each data point [36]. The ratio of the unfolded spectrum from each iteration to that of the primary analysis is calculated, and at each point the median of this set of ratios is assigned as the systematic uncertainty from this source.

Tables 1 and 2 show representative values of the systematic uncertainty in $\Delta_{\text{recoil}}(p_{\text{T,jet}}^{\text{ch}})$ and $\Delta_{\text{recoil}}(\Delta\phi)$ measurements for MB and HM-selected event populations, respectively.

Table 1: Main sources of systematic uncertainty and total uncertainty in $\Delta_{\text{recoil}}(p_{\text{T,jet}}^{\text{ch}})$ and $\Delta_{\text{recoil}}(\Delta\phi)$ in representative bins, for MB events.

Projection	Relative systematic uncertainty (%)					
	$\Delta_{\text{recoil}}(p_{\text{T,jet}}^{\text{ch}})$ $ \Delta\phi - \pi < 0.6$		$\Delta_{\text{recoil}}(\Delta\phi)$ $p_{\text{T,jet}}^{\text{ch}} \in (20, 40)$ GeV/c		$\Delta_{\text{recoil}}(\Delta\phi)$ $p_{\text{T,jet}}^{\text{ch}} \in (40, 60)$ GeV/c	
	Bin	10–20 GeV/c	60–80 GeV/c	$2\pi/3$	π	$2\pi/3$
Tracking efficiency	0.2	7.1	3.7	1.9	8.4	5.6
Track p_{T} resolution	0.3	0.3	0.2	0.2	~ 0	0.3
Unfolding procedure	0.6	0.7	3.9	0.3	3.4	0.9
c_{Ref} variation	(-1.7, 1.9)	(-0.2, 0.2)	(-0.6, 0.7)	(-0.4, 0.4)	(-0.5, 0.5)	(-0.1, 0.2)
Bkgd fluctuations	(-1.6, 0)	(-2.4, 0)	(-4.7, 0)	(-1.6, 0)	(-5.0, 0)	(-2.7, 0)
Total uncertainty	(-2.5, 2.0)	(-7.6, 7.2)	(-7.2, 5.4)	(-2.5, 2.0)	(-10.4, 9.0)	(-6.3, 5.7)

Table 2: Same as Tab. 1, for HM-selected events.

Projection	Relative systematic uncertainty (%)					
	$\Delta_{\text{recoil}}(p_{\text{T,jet}}^{\text{ch}})$ $ \Delta\phi - \pi < 0.6$		$\Delta_{\text{recoil}}(\Delta\phi)$ $p_{\text{T,jet}}^{\text{ch}} \in (20, 40)$ GeV/c		$\Delta_{\text{recoil}}(\Delta\phi)$ $p_{\text{T,jet}}^{\text{ch}} \in (40, 60)$ GeV/c	
	Bin	10–20 GeV/c	60–80 GeV/c	$2\pi/3$	π	$2\pi/3$
Tracking efficiency	0.6	7.6	4.2	1.9	7.1	5.2
Track p_{T} resolution	0.3	0.1	0.4	0.2	0.1	0.3
Unfolding procedure	0.9	0.7	5.7	1.6	2.6	1.2
c_{Ref} variation	(-4.5, 3.2)	(-0.3, 0.2)	(-1.5, 1.1)	(-0.6, 0.5)	(-1.3, 0.9)	(-0.3, 0.2)
Bkgd fluctuations	(-1.5, 0)	(-3.0, 0)	(-7.4, 0)	(-2.1, 0)	(-4.5, 0)	(-3.2, 0)
Total uncertainty	(-4.6, 3.7)	(-8.2, 7.6)	(-10.3, 7.2)	(-3.3, 2.5)	(-8.9, 7.6)	(-6.3, 5.4)

7.1 Tracking efficiency and track p_{T} resolution

The tracking efficiency uncertainty is 3% [56]. To assess the corresponding uncertainty in the Δ_{recoil} distribution, a variation of R_{instr} is constructed in which 3% of all tracks are randomly discarded. While it is in practice not possible to generate R_{instr} with 3% higher tracking efficiency, this uncertainty is expected to be symmetric. The resulting uncertainty ranges from $< 1\%$ at low $p_{\text{T,jet}}^{\text{ch}}$ to 7% at high $p_{\text{T,jet}}^{\text{ch}}$, with only minor dependence on EA.

To assess the systematic uncertainty due to track p_{T} resolution, two different instances of R_{instr} are generated, with p_{T} -resolution corresponding to that of either real data or detector-level MC data hybrid tracks. This source makes negligible contribution to the total systematic uncertainty.

7.2 Unfolding

The unfolding procedure has several parameters whose values influence the corrected Δ_{recoil} distribution: number of iterations; choice of prior spectrum; and range and binning of the raw input distribution. Each source was varied independently:

- The regularization condition was varied by ± 1 iterations with respect to the optimized value of 5. The corresponding uncertainty is found to be small, since unfolding converges rapidly to a stable result.

- Variations in the prior spectrum were obtained using the particle-level Δ_{recoil} spectra generated by the POWHEG MC event generator [70, 71] matched to PYTHIA 8 for parton shower and hadronization, and with different choices of regularization and factorization scale.
- The $p_{T,\text{jet}}$ binning was varied by shifting the bin boundaries by 1–2 GeV/ c , and by changing the lower bound of the input spectrum from 10 GeV/ c to 6 GeV/ c . The binning in $\Delta\phi$ was not varied, since $\Delta\phi$ smearing effects are small.

The systematic uncertainty attributed to unfolding is the maximum deviation in the Δ_{recoil} spectrum from varying these parameters, relative to the Δ_{recoil} spectrum using the primary analysis parameters. For $\Delta_{\text{recoil}}(p_{T,\text{jet}}^{\text{ch}})$, the resulting relative systematic uncertainty is about 0.6% for MB and 0.9% for HM events, with a weak dependence on $p_{T,\text{jet}}^{\text{ch}}$. For $\Delta_{\text{recoil}}(\Delta\phi)$, the relative systematic uncertainty is smallest at $\Delta\phi = \pi$ and increases monotonically towards $\Delta\phi = \pi/2$, for both MB and HM events.

7.3 Scaling factor c_{Ref}

The value of the c_{Ref} scaling factor in Eq. 3 was varied in the range [0.9, 1]. This range brackets the c_{Ref} values obtained by changing the $p_{T,\text{jet}}^{\text{reco,ch}}$ bin in which it is evaluated from (0, 1) GeV/ c to (–1, 0) GeV/ c , and by its variation with $\Delta\phi$. Different choices of c_{Ref} modify the Δ_{recoil} spectrum relative to that of the primary analysis result, with uncertainty decreasing as a function of $p_{T,\text{jet}}^{\text{ch}}$. Representative values are provided in Tables 1 and 2.

7.4 Background fluctuations

As discussed in Sec. 6, no correction is applied directly for the effect of residual background fluctuations; rather, a model-dependent estimate of its magnitude contributes to the systematic uncertainty. For this estimate, a response matrix which encodes the effect of residual background fluctuations, R_{bkgd} , is convoluted with the instrumental response matrix R_{instr} in Eq. 4. The matrix R_{bkgd} is determined for events selected with TT{20, 30}, using two methods:

- Calculate the sum of track p_T in a cone $R = 0.4$ placed randomly in the acceptance, excluding overlap with the leading and sub-leading jets, and the TT. This sum is corrected for the median background density,

$$\delta p_T^{\text{RC}} = \sum_{\text{tracks} \in \text{RC}} p_{T,\text{track}} - \rho \times \pi R^2, \quad (5)$$

where πR^2 is the cone area and ρ is defined in Eq. 1. The matrix R_{bkgd} is the distribution of δp_T^{RC} .

- Embed a high- p_T track perpendicular in azimuth to the TT and at the same value of η , with p_T distributed uniformly in the range 0–20 GeV/ c . Jet reconstruction is then carried out, the jet candidate containing the embedded track is identified, and the quantity δp_T^{ET} is calculated as

$$\delta p_T^{\text{ET}} = p_{T,\text{jet}}^{\text{ch,emb}} - \rho \times A_{\text{jet}}^{\text{emb}} - p_T^{\text{emb}}, \quad (6)$$

where p_T^{emb} is transverse momentum of the embedded track. The matrix R_{bkgd} is the distribution of δp_T^{ET} .

Unfolding is then carried out for both choices, and the assigned systematic uncertainty is the maximum difference of the two unfolded Δ_{recoil} distributions from that of the primary analysis.

7.5 Total systematic uncertainty

The total systematic uncertainty of the unfolded Δ_{recoil} distribution is the quadrature sum of the contribution from each source. The systematic uncertainties from all sources except unfolding are correlated between the HM and MB analyses. This correlation is accounted for in the systematic uncertainty of ratios of Δ_{recoil} distributions by estimating the systematic uncertainty directly from the spread of the ratios calculated for each variation of the analysis configuration.

8 Results

8.1 Fully corrected distributions

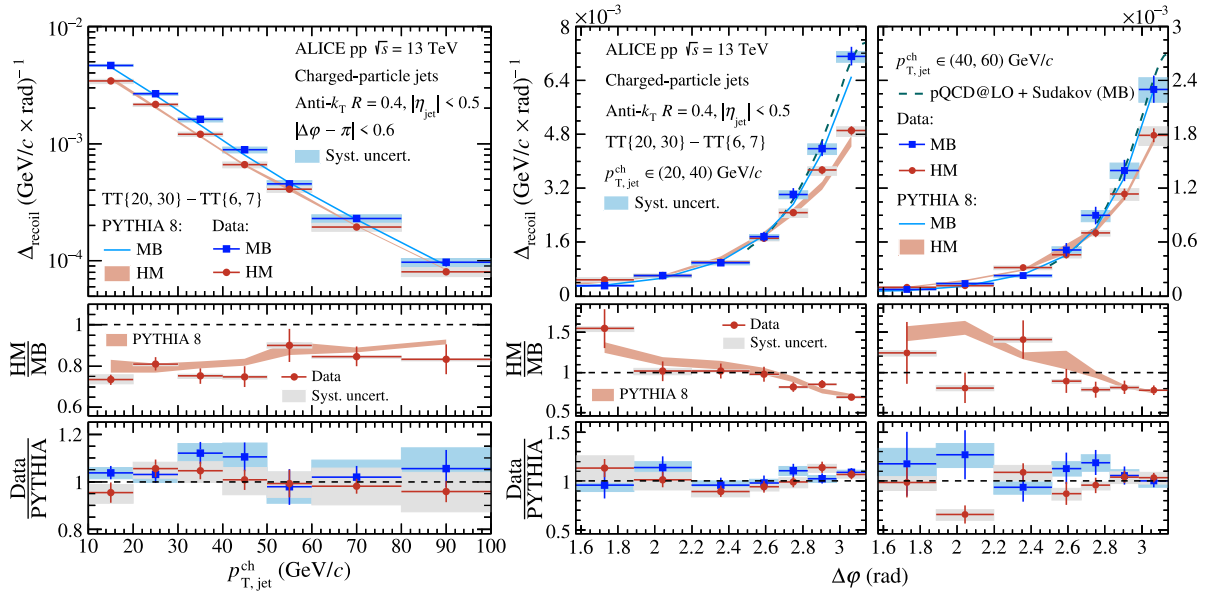


Figure 3: Fully-corrected Δ_{recoil} distributions measured in MB and HM-selected events in pp collisions at $\sqrt{s} = 13$ TeV. Left panel: $\Delta_{\text{recoil}}(p_{T,\text{jet}}^{\text{ch}})$ in $|\Delta\phi - \pi| < 0.6$; middle and right panels: $\Delta_{\text{recoil}}(\Delta\phi)$ for $20 < p_{T,\text{jet}}^{\text{ch}} < 40$ GeV/c and $40 < p_{T,\text{jet}}^{\text{ch}} < 60$ GeV/c. Also shown are particle-level simulated distributions calculated with PYTHIA 8 Monash tune, and a pQCD calculation at LO with Sudakov broadening [51, 72, 73] (MB $\Delta_{\text{recoil}}(\Delta\phi)$ only). The width of the PYTHIA 8 HM band represents the statistical uncertainty. Top row: Δ_{recoil} distributions; middle row: ratio of Δ_{recoil} distributions for HM/MB from data; bottom row: Data/PYTHIA 8 separately for MB and HM event selections.

Figure 3 shows fully-corrected distributions of $\Delta_{\text{recoil}}(p_{T,\text{jet}}^{\text{ch}})$ and $\Delta_{\text{recoil}}(\Delta\phi)$ measured in MB and HM-selected pp collisions at $\sqrt{s} = 13$ TeV, together with calculations based on PYTHIA 8, Monash tune, and a pQCD calculation at LO with Sudakov broadening [51, 72, 73] (the latter only for $\Delta_{\text{recoil}}(\Delta\phi)$ in MB collisions). Since the pQCD calculation is LO, there are large uncertainties in its normalization; the $\Delta_{\text{recoil}}(\Delta\phi)$ distributions from the calculation are therefore scaled to the integrated yield of the data in the same $p_{T,\text{jet}}^{\text{ch}}$ bin in order to compare their shapes. Both PYTHIA 8 and the pQCD calculation ($\Delta_{\text{recoil}}(\Delta\phi)$ shape only) are consistent with the distributions measured in MB events, within experimental uncertainties.

Comparison of the MB and HM $\Delta_{\text{recoil}}(p_{T,\text{jet}}^{\text{ch}})$ distributions reveals a yield suppression in HM collisions that is largely independent of $p_{T,\text{jet}}$, though there is a hint of a harder recoil jet spectrum for HM events. The mean value of the yield ratio HM/MB in the left panel of Fig. 3 is 0.78. The $\Delta_{\text{recoil}}(\Delta\phi)$ distributions show that the jet-yield suppression in HM events occurs predominantly in the back-to-back configuration, with the yield ratio HM/MB in the bin $\Delta\phi \sim \pi$ measured to be 0.69 for $20 < p_{T,\text{jet}}^{\text{ch}} < 40$ GeV/c (Fig. 3, middle panel) and 0.78 for $40 < p_{T,\text{jet}}^{\text{ch}} < 60$ GeV/c (Fig. 3, left panel). The total yield is suppressed, while

the azimuthal distribution is broadened; such broadening could arise from jet quenching, i.e. medium-induced jet scattering occurs preferentially in HM events. Notably, however, PYTHIA 8 particle-level distributions likewise exhibit jet yield suppression and azimuthal broadening for HM-selected events, accurately reproducing the measured distributions. Since PYTHIA 8 does not incorporate jet quenching, this disfavors jet quenching as the predominant effect generating the broadening seen in data.

8.2 Origin of HM induced TT-jet acoplanarity in PYTHIA 8

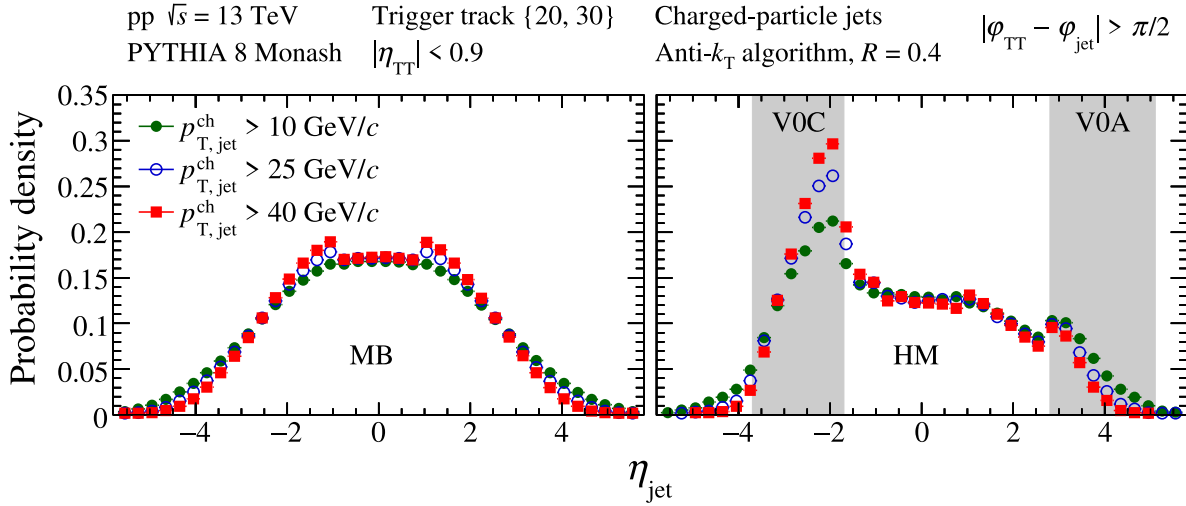


Figure 4: PYTHIA 8 particle-level simulation of the probability distribution of the yield of charged-particle jets ($R = 0.4$) recoiling from a high- p_T hadron (TT{20,30}) as a function of η_{jet} for various $p_{T,\text{jet}}^{\text{ch}}$ intervals, in pp collisions at $\sqrt{s} = 13$ TeV. Left: MB events; right: HM events. V0A and V0C acceptances are also shown.

To clarify the origin of the broadening, a more detailed investigation is carried out using both data and particle-level distributions from PYTHIA 8 simulations.

Figure 4 shows the calculated pseudorapidity (η_{jet}) distribution of charged-particle jets recoiling from a high- p_T trigger hadron with TT{20,30} in MB and HM-selected event populations, for various lower thresholds in $p_{T,\text{jet}}^{\text{ch}}$. Since the per-trigger yield varies with $p_{T,\text{jet}}^{\text{ch}}$, these distributions are normalized to unit integral to enable a direct comparison of their shapes. The acceptances of V0A and V0C are also shown; note that V0C covers smaller values of $|\eta|$ than V0A. While the η_{jet} distribution for MB events is symmetric, the η_{jet} distribution for HM events is highly asymmetric, with significant enhancement in the relative rate of recoil jets in the V0C acceptance. The enhancement is largest for the highest value of $p_{T,\text{jet}}^{\text{ch}}$.

Figure 5 shows similar distributions for recoil jets with $p_{T,\text{jet}}^{\text{ch}} > 25$ GeV/ c , in various intervals of V0M/⟨V0M⟩. A striking enhancement is observed in the per-trigger jet yield within the V0C acceptance for the largest values of V0M/⟨V0M⟩. Since HM events are selected based on the value of V0M/⟨V0M⟩, it is evident that the HM selection induces a bias which enhances the rate of hard recoil jets in the V0C acceptance.

Figure 6 provides additional insight into the bias induced by the HM event selection. The figure shows the probability to observe a specific number of jets with $R = 0.4$ and $p_{T,\text{jet}}^{\text{ch}} > 15$ GeV/ c recoiling against a high- p_T hadron trigger (TT{20,30}) in the ALICE central barrel acceptance ($|\eta_{\text{jet}}| < 0.5$), for MB and HM pp collisions at $\sqrt{s} = 13$ TeV. Distributions are shown for both data and PYTHIA 8 calculations.

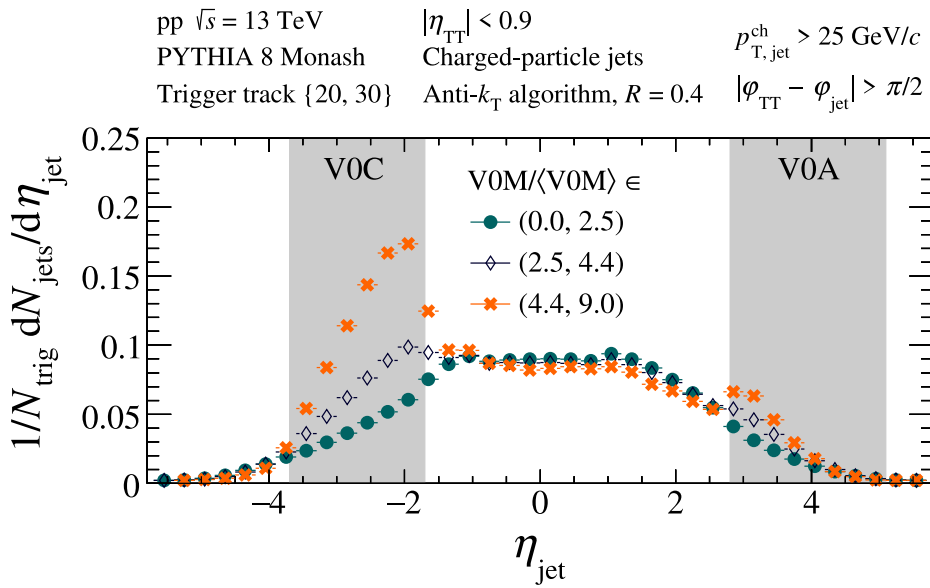


Figure 5: Same as Fig. 4, but for recoil jets with $p_{\text{T,jet}}^{\text{ch}} > 25$ GeV/c for various intervals in $V0M/\langle V0M \rangle$. Distributions are normalized per trigger.

In both data and simulations, the probability to observe a single jet is suppressed in HM relative to MB events by 2–3%, while the probability to observe multiple jets is significantly enhanced.

The effect of the HM selection bias shown in Figs. 4, 5 and 6 on the acoplanarity distributions in Fig. 3 can be understood as follows. The HM requirement preferentially selects events with a recoil jet in the V0C acceptance. For the leading-order (LO) di-jet channel, in which the TT and recoil jet are azimuthally back-to-back, this depletes both the per-trigger rate for recoil jets observed in the central barrel ($|\eta_{\text{jet}}| < 0.9 - R$) at $\Delta\varphi \sim \pi$ and the relative rate of single recoil jets in the acceptance. The recoil jets observed in the ALICE central barrel in HM events therefore arise at enhanced rate from higher-order production processes, with multiple recoil jets in the final state. These jets from higher-order processes have broader distribution in $\Delta\varphi$ than jets from LO production. This picture is confirmed by carrying out the PYTHIA 8 analysis for much larger recoil jet acceptance, $|\eta_{\text{jet}}| < 5.6$. In that case, no back-to-back yield depletion is observed.

The yield suppression and azimuthal broadening seen in Fig. 3 may therefore arise from the effect of different phase space being used for EA characterization (V0A and V0C) and recoil jet measurement (central barrel), combined with the HM selection bias towards events with a jet in the V0C acceptance. It therefore cannot be attributed uniquely to jet quenching in HM-selected events.

This conclusion about interpretability in terms of jet quenching of the effects seen in Fig. 3 is more general than this specific analysis, however. The bias of the HM event selection identified here is generic, and must also be taken into account for the interpretation in terms of QGP formation of other phenomena observed in small systems.

9 Summary

This article reports a search for jet quenching effects in high multiplicity pp collisions at $\sqrt{s} = 13$ TeV, based on the semi-inclusive azimuthal distribution of charged-particle jets recoiling from a high- p_T hadron trigger in the ALICE central barrel acceptance. Significant azimuthal broadening is observed in events selected to have high multiplicity in forward detectors, which may arise from jet quenching. However, similar broadening is also observed in simulations with the PYTHIA 8 event generator, which

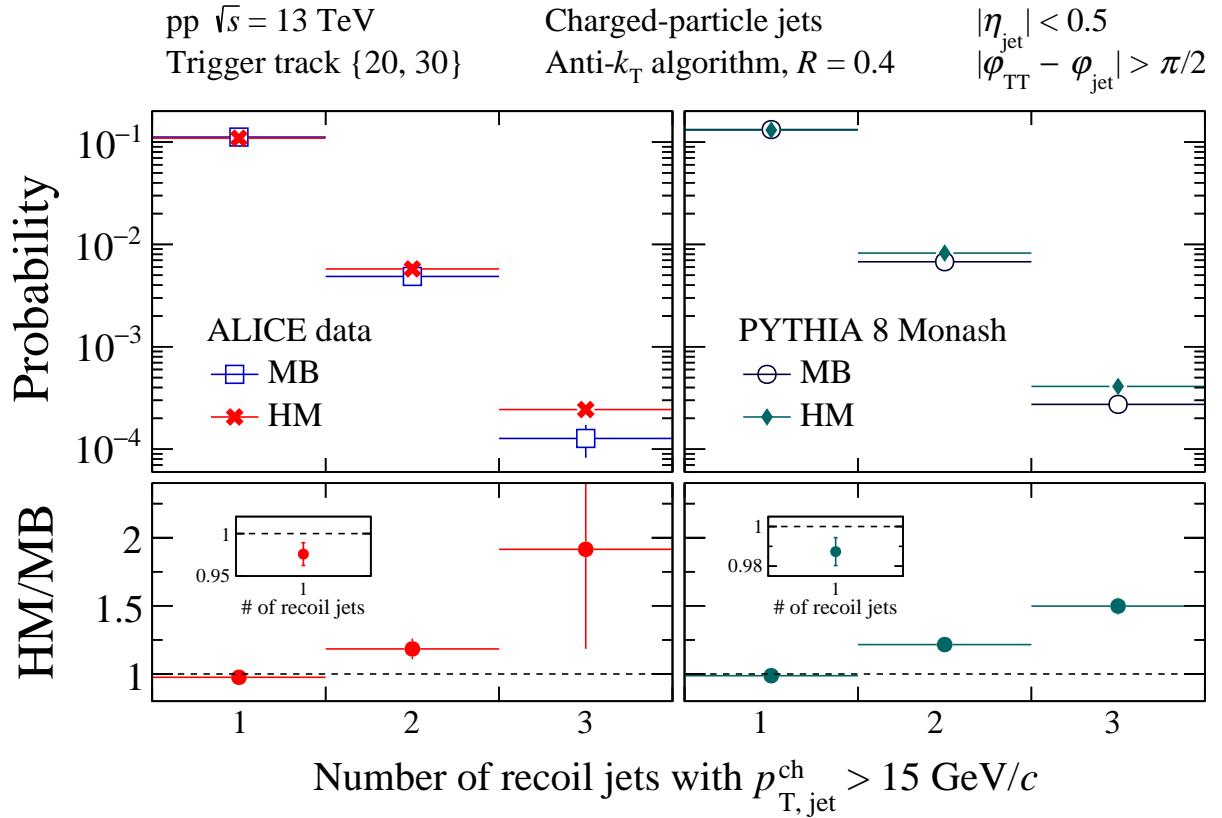


Figure 6: Distribution of probability per trigger hadron of number of jets with $R = 0.4$ and $p_{T, \text{jet}}^{\text{ch}} > 15$ GeV/ c recoiling from a high- p_T hadron (TT{20, 30}) at midrapidity ($|\eta_{\text{jet}}| < 0.5$), for MB and HM pp collisions at $\sqrt{s} = 13$ TeV. Left panels: ALICE data; right panels: simulations at the particle level with PYTHIA 8 Monash tune. Lower panels show the ratio HM/MB. The insert in the lower panels has magnified vertical scale to show the ratio of probabilities to observe a single jet.

does not incorporate jet quenching.

Detailed analysis of the data and simulations reveals that the high-multiplicity event selection, which is based on the V0 detectors at forward and backward rapidities, preferentially selects events with an energetic jet in the forward detector, consequently biasing the acoplanarity distribution measured in the central region. We conclude that this observable is therefore not uniquely sensitive to jet quenching effects in small collision systems. This bias is generic, however, and it should likewise be taken into account in the interpretation of other measurements which probe the formation of a quasi-equilibrated quark–gluon plasma in small collision systems.

Acknowledgements

The ALICE Collaboration would like to thank all its engineers and technicians for their invaluable contributions to the construction of the experiment and the CERN accelerator teams for the outstanding performance of the LHC complex. The ALICE Collaboration gratefully acknowledges the resources and support provided by all Grid centres and the Worldwide LHC Computing Grid (WLCG) collaboration. The ALICE Collaboration acknowledges the following funding agencies for their support in building and running the ALICE detector: A. I. Alikhanyan National Science Laboratory (Yerevan Physics Institute) Foundation (ANSL), State Committee of Science and World Federation of Scientists (WFS), Armenia; Austrian Academy of Sciences, Austrian Science Fund (FWF): [M 2467-N36] and Nationalstiftung für Forschung, Technologie und Entwicklung, Austria; Ministry of Communications and High

Technologies, National Nuclear Research Center, Azerbaijan; Conselho Nacional de Desenvolvimento Científico e Tecnológico (CNPq), Financiadora de Estudos e Projetos (Finep), Fundação de Amparo à Pesquisa do Estado de São Paulo (FAPESP) and Universidade Federal do Rio Grande do Sul (UFRGS), Brazil; Bulgarian Ministry of Education and Science, within the National Roadmap for Research Infrastructures 2020-2027 (object CERN), Bulgaria; Ministry of Education of China (MOEC), Ministry of Science & Technology of China (MSTC) and National Natural Science Foundation of China (NSFC), China; Ministry of Science and Education and Croatian Science Foundation, Croatia; Centro de Aplicaciones Tecnológicas y Desarrollo Nuclear (CEADEN), Cubaenergía, Cuba; Ministry of Education, Youth and Sports of the Czech Republic, Czech Republic; The Danish Council for Independent Research | Natural Sciences, the VILLUM FONDEN and Danish National Research Foundation (DNRF), Denmark; Helsinki Institute of Physics (HIP), Finland; Commissariat à l’Energie Atomique (CEA) and Institut National de Physique Nucléaire et de Physique des Particules (IN2P3) and Centre National de la Recherche Scientifique (CNRS), France; Bundesministerium für Bildung und Forschung (BMBF) and GSI Helmholtzzentrum für Schwerionenforschung GmbH, Germany; General Secretariat for Research and Technology, Ministry of Education, Research and Religions, Greece; National Research, Development and Innovation Office, Hungary; Department of Atomic Energy Government of India (DAE), Department of Science and Technology, Government of India (DST), University Grants Commission, Government of India (UGC) and Council of Scientific and Industrial Research (CSIR), India; National Research and Innovation Agency - BRIN, Indonesia; Istituto Nazionale di Fisica Nucleare (INFN), Italy; Japanese Ministry of Education, Culture, Sports, Science and Technology (MEXT) and Japan Society for the Promotion of Science (JSPS) KAKENHI, Japan; Consejo Nacional de Ciencia (CONACYT) y Tecnología, through Fondo de Cooperación Internacional en Ciencia y Tecnología (FONCICYT) and Dirección General de Asuntos del Personal Académico (DGAPA), Mexico; Nederlandse Organisatie voor Wetenschappelijk Onderzoek (NWO), Netherlands; The Research Council of Norway, Norway; Commission on Science and Technology for Sustainable Development in the South (COMSATS), Pakistan; Pontificia Universidad Católica del Perú, Peru; Ministry of Education and Science, National Science Centre and WUT ID-UB, Poland; Korea Institute of Science and Technology Information and National Research Foundation of Korea (NRF), Republic of Korea; Ministry of Education and Scientific Research, Institute of Atomic Physics, Ministry of Research and Innovation and Institute of Atomic Physics and Universitatea Nationala de Stiinta si Tehnologie Politehnica Bucuresti, Romania; Ministry of Education, Science, Research and Sport of the Slovak Republic, Slovakia; National Research Foundation of South Africa, South Africa; Swedish Research Council (VR) and Knut & Alice Wallenberg Foundation (KAW), Sweden; European Organization for Nuclear Research, Switzerland; Suranaree University of Technology (SUT), National Science and Technology Development Agency (NSTDA) and National Science, Research and Innovation Fund (NSRF via PMU-B B05F650021), Thailand; Turkish Energy, Nuclear and Mineral Research Agency (TENMAK), Turkey; National Academy of Sciences of Ukraine, Ukraine; Science and Technology Facilities Council (STFC), United Kingdom; National Science Foundation of the United States of America (NSF) and United States Department of Energy, Office of Nuclear Physics (DOE NP), United States of America. In addition, individual groups or members have received support from: Czech Science Foundation (grant no. 23-07499S), Czech Republic; European Research Council, Strong 2020 - Horizon 2020 (grant nos. 950692, 824093), European Union; ICSC - Centro Nazionale di Ricerca in High Performance Computing, Big Data and Quantum Computing, European Union - NextGenerationEU; Academy of Finland (Center of Excellence in Quark Matter) (grant nos. 346327, 346328), Finland.

References

- [1] W. Busza, K. Rajagopal, and W. van der Schee, “Heavy Ion Collisions: The Big Picture, and the Big Questions”, *Ann. Rev. Nucl. Part. Sci.* **68** (2018) 339–376, arXiv:1802.04801 [hep-ph].

- [2] **ALICE** Collaboration, “The ALICE experiment – A journey through QCD”, arXiv:2211.04384 [nucl-ex].
- [3] U. Heinz and R. Snellings, “Collective flow and viscosity in relativistic heavy-ion collisions”, *Ann. Rev. Nucl. Part. Sci.* **63** (2013) 123–151, arXiv:1301.2826 [nucl-th].
- [4] **ALICE** Collaboration, J. Adam *et al.*, “Centrality dependence of particle production in p–Pb collisions at $\sqrt{s_{NN}} = 5.02$ TeV”, *Phys. Rev. C* **91** (2015) 064905, arXiv:1412.6828 [nucl-ex].
- [5] J. L. Nagle and W. A. Zajc, “Small System Collectivity in Relativistic Hadronic and Nuclear Collisions”, *Ann. Rev. Nucl. Part. Sci.* **68** (2018) 211–235, arXiv:1801.03477 [nucl-ex].
- [6] **CMS** Collaboration, V. Khachatryan *et al.*, “Observation of Long-Range Near-Side Angular Correlations in Proton-Proton Collisions at the LHC”, *JHEP* **1009** (2010) 091, arXiv:1009.4122 [nucl-ex].
- [7] **ALICE** Collaboration, B. Abelev *et al.*, “Long-range angular correlations on the near and away side in p–Pb collisions at $\sqrt{s_{NN}} = 5.02$ TeV”, *Phys. Lett. B* **719** (2013) 29–41, arXiv:1212.2001 [nucl-ex].
- [8] **PHENIX** Collaboration, C. Aidala *et al.*, “Creation of quark–gluon plasma droplets with three distinct geometries”, *Nature Phys.* **15** (2019) 214–220, arXiv:1805.02973 [nucl-ex].
- [9] **STAR** Collaboration, M. I. Abdulhamid *et al.*, “Measurements of the Elliptic and Triangular Azimuthal Anisotropies in Central $^3\text{He}+\text{Au}$, $\text{d}+\text{Au}$ and $\text{p}+\text{Au}$ Collisions at $\sqrt{s_{NN}} = 200$ GeV”, *Phys. Rev. Lett.* **130** (2023) 242301, arXiv:2210.11352 [nucl-ex].
- [10] **ALICE** Collaboration, J. Adam *et al.*, “Enhanced production of multi-strange hadrons in high-multiplicity proton–proton collisions”, *Nature Phys.* **13** (2017) 535–539, arXiv:1606.07424 [nucl-ex].
- [11] **CMS** Collaboration, V. Khachatryan *et al.*, “Measurement of the double-differential inclusive jet cross section in proton–proton collisions at $\sqrt{s} = 13$ TeV”, *Eur. Phys. J. C* **76** (2016) 451, arXiv:1605.04436 [hep-ex].
- [12] **ATLAS** Collaboration, M. Aaboud *et al.*, “Measurement of inclusive jet and dijet cross-sections in proton–proton collisions at $\sqrt{s} = 13$ TeV with the ATLAS detector”, *JHEP* **05** (2018) 195, arXiv:1711.02692 [hep-ex].
- [13] **ALICE** Collaboration, S. Acharya *et al.*, “Measurements of inclusive jet spectra in pp and central Pb–Pb collisions at $\sqrt{s_{NN}} = 5.02$ TeV”, *Phys. Rev. C* **101** (2020) 034911, arXiv:1909.09718 [nucl-ex].
- [14] A. Majumder and M. Van Leeuwen, “The Theory and Phenomenology of Perturbative QCD Based Jet Quenching”, *Prog. Part. Nucl. Phys. A* **66** (2011) 41–92, arXiv:1002.2206 [hep-ph].
- [15] L. Cunqueiro and A. M. Sickles, “Studying the QGP with Jets at the LHC and RHIC”, *Prog. Part. Nucl. Phys.* **124** (2022) 103940, arXiv:2110.14490 [nucl-ex].
- [16] X. Zhang and J. Liao, “Jet Quenching and Its Azimuthal Anisotropy in AA and possibly High Multiplicity pA and dA Collisions”, arXiv:1311.5463 [nucl-th].
- [17] K. Tywoniuk, “Is there jet quenching in pPb?”, *Nucl. Phys. A* **926** (2014) 85–91.
- [18] C. Park, C. Shen, S. Jeon, and C. Gale, “Rapidity-dependent jet energy loss in small systems with finite-size effects and running coupling”, *Nucl. Part. Phys. Proc.* **289–290** (2017) 289–292, arXiv:1612.06754 [nucl-th].
- [19] A. Huss, A. Kurkela, A. Mazeliauskas, R. Paatelainen, W. van der Schee, and U. A. Wiedemann, “Predicting parton energy loss in small collision systems”, *Phys. Rev. C* **103** (2021) 054903, arXiv:2007.13758 [hep-ph].
- [20] A. Huss, A. Kurkela, A. Mazeliauskas, R. Paatelainen, W. van der Schee, and U. A. Wiedemann, “Discovering Partonic Rescattering in Light Nucleus Collisions”, *Phys. Rev. Lett.* **126** (2021) 192301, arXiv:2007.13754 [hep-ph].

- [21] B. G. Zakharov, “Jet quenching from heavy to light ion collisions”, *JHEP* **09** (2021) 087, arXiv:2105.09350 [hep-ph].
- [22] W. Ke and I. Vitev, “Searching for QGP droplets with high- p_T hadrons and heavy flavor”, *Phys. Rev. C* **107** (2023) 064903, arXiv:2204.00634 [hep-ph].
- [23] M. L. Miller, K. Reygers, S. J. Sanders, and P. Steinberg, “Glauber modeling in high energy nuclear collisions”, *Ann. Rev. Nucl. Part. Sci.* **57** (2007) 205–243, arXiv:nucl-ex/0701025 [nucl-ex].
- [24] **PHENIX** Collaboration, A. Adare *et al.*, “Centrality-dependent modification of jet-production rates in deuteron-gold collisions at $\sqrt{s_{NN}} = 200$ GeV”, *Phys. Rev. Lett.* **116** (2016) 122301, arXiv:1509.04657 [nucl-ex].
- [25] **ATLAS** Collaboration, G. Aad *et al.*, “Centrality and rapidity dependence of inclusive jet production in $\sqrt{s_{NN}} = 5.02$ TeV proton-lead collisions with the ATLAS detector”, *Phys. Lett. B* **748** (2015) 392–413, arXiv:1412.4092 [hep-ex].
- [26] **PHENIX** Collaboration, A. Adare *et al.*, “Centrality categorization for $R_{p(d)+A}$ in high-energy collisions”, *Phys. Rev. C* **90** (2014) 034902, arXiv:1310.4793 [nucl-ex].
- [27] M. Alvioli, B. A. Cole, L. Frankfurt, D. V. Perepelitsa, and M. Strikman, “Evidence for x -dependent proton color fluctuations in pA collisions at the CERN Large Hadron Collider”, *Phys. Rev. C* **93** (2016) 011902, arXiv:1409.7381 [hep-ph].
- [28] A. Bzdak, V. Skokov, and S. Bathe, “Centrality dependence of high energy jets in p+Pb collisions at energies available at the CERN Large Hadron Collider”, *Phys. Rev. C* **93** (2016) 044901, arXiv:1408.3156 [hep-ph].
- [29] M. Kordell and A. Majumder, “Jets in d(p)-A Collisions: Color Transparency or Energy Conservation”, *Phys. Rev. C* **97** (2018) 054904, arXiv:1601.02595 [nucl-th].
- [30] C. Loizides and A. Morsch, “Absence of jet quenching in peripheral nucleus–nucleus collisions”, *Phys. Lett. B* **773** (2017) 408–411, arXiv:1705.08856 [nucl-ex].
- [31] M. Alvioli, L. Frankfurt, D. Perepelitsa, and M. Strikman, “Global analysis of color fluctuation effects in proton– and deuteron–nucleus collisions at RHIC and the LHC”, *Phys. Rev. D* **98** (2018) 071502, arXiv:1709.04993 [hep-ph].
- [32] **PHENIX** Collaboration, N. J. Abdulameer *et al.*, “Disentangling centrality bias and final-state effects in the production of high- p_T π^0 using direct γ in d–Au collisions at $\sqrt{s_{NN}} = 200$ GeV”, arXiv:2303.12899 [nucl-ex].
- [33] **ALICE** Collaboration, S. Acharya *et al.*, “Measurement of prompt D^0 , D^+ , D^{*+} , and D_s^+ production in p–Pb collisions at $\sqrt{s_{NN}} = 5.02$ TeV”, *JHEP* **12** (2019) 092, arXiv:1906.03425 [nucl-ex].
- [34] **ALICE** Collaboration, S. Acharya *et al.*, “Nuclear modification factor of light neutral-meson spectra up to high transverse momentum in p–Pb collisions at $\sqrt{s_{NN}} = 8.16$ TeV”, *Phys. Lett. B* **827** (2022) 136943, arXiv:2104.03116 [nucl-ex].
- [35] **ALICE** Collaboration, S. Acharya *et al.*, “Measurement of inclusive charged-particle b-jet production in pp and p–Pb collisions at $\sqrt{s_{NN}} = 5.02$ TeV”, *JHEP* **01** (2022) 178, arXiv:2110.06104 [nucl-ex].
- [36] **ALICE** Collaboration, S. Acharya *et al.*, “Constraints on jet quenching in p–Pb collisions at $\sqrt{s_{NN}} = 5.02$ TeV measured by the event-activity dependence of semi-inclusive hadron-jet distributions”, *Phys. Lett. B* **783** (2018) 95–113, arXiv:1712.05603 [nucl-ex].
- [37] **ATLAS** Collaboration, G. Aad *et al.*, “Strong constraints on jet quenching in centrality-dependent p+Pb collisions at 5.02 TeV from ATLAS”, *Phys. Rev. Lett.* **131** (2023) 072301, arXiv:2206.01138 [nucl-ex].
- [38] **ATLAS** Collaboration, G. Aad *et al.*, “Transverse momentum and process dependent azimuthal

- anisotropies in $\sqrt{s_{NN}} = 8.16$ TeV p +Pb collisions with the ATLAS detector”, *Eur. Phys. J. C* **80** (2020) 73, arXiv:1910.13978 [nucl-ex].
- [39] L. Yan and J.-Y. Ollitrault, “Universal fluctuation-driven eccentricities in proton-proton, proton-nucleus and nucleus-nucleus collisions”, *Phys. Rev. Lett.* **112** (2014) 082301, arXiv:1312.6555 [nucl-th].
- [40] C. Bierlich, G. Gustafson, and L. Lönnblad, “Collectivity without plasma in hadronic collisions”, *Phys. Lett. B* **779** (2018) 58–63, arXiv:1710.09725 [hep-ph].
- [41] B. Blok, C. D. Jäkel, M. Strikman, and U. A. Wiedemann, “Collectivity from interference”, *JHEP* **12** (2017) 074, arXiv:1708.08241 [hep-ph].
- [42] ALICE Collaboration, J. Adam *et al.*, “Measurement of jet quenching with semi-inclusive hadron-jet distributions in central Pb–Pb collisions at $\sqrt{s_{NN}} = 2.76$ TeV”, *JHEP* **09** (2015) 170, arXiv:1506.03984 [nucl-ex].
- [43] STAR Collaboration, L. Adamczyk *et al.*, “Measurements of jet quenching with semi-inclusive hadron+jet distributions in Au+Au collisions at $\sqrt{s_{NN}} = 200$ GeV”, *Phys. Rev. C* **96** (2017) 024905, arXiv:1702.01108 [nucl-ex].
- [44] ALICE Collaboration, S. Acharya *et al.*, “Observation of medium-induced yield enhancement and acoplanarity broadening of low- p_T jets from measurements in pp and central Pb–Pb collisions at $\sqrt{s_{NN}} = 5.02$ TeV”, arXiv:2308.16131 [nucl-ex].
- [45] ALICE Collaboration, S. Acharya *et al.*, “Measurements of jet quenching using semi-inclusive hadron+jet distributions in pp and central Pb–Pb collisions at $\sqrt{s_{NN}} = 5.02$ TeV”, arXiv:2308.16128 [nucl-ex].
- [46] M. Cacciari, G. P. Salam, and G. Soyez, “The anti- k_t jet clustering algorithm”, *JHEP* **04** (2008) 063, arXiv:0802.1189 [hep-ph].
- [47] D. A. Appel, “Jets as a Probe of Quark - Gluon Plasmas”, *Phys. Rev. D* **33** (1986) 717.
- [48] J. P. Blaizot and L. D. McLerran, “Jets in Expanding Quark - Gluon Plasmas”, *Phys. Rev. D* **34** (1986) 2739.
- [49] F. D’Eramo, H. Liu, and K. Rajagopal, “Transverse Momentum Broadening and the Jet Quenching Parameter, Redux”, *Phys. Rev. D* **84** (2011) 065015, arXiv:1006.1367 [hep-ph].
- [50] F. D’Eramo, M. Lekaveckas, H. Liu, and K. Rajagopal, “Momentum Broadening in Weakly Coupled Quark-Gluon Plasma (with a view to finding the quasiparticles within liquid quark-gluon plasma)”, *JHEP* **05** (2013) 031, arXiv:1211.1922 [hep-ph].
- [51] L. Chen, G.-Y. Qin, S.-Y. Wei, B.-W. Xiao, and H.-Z. Zhang, “Probing Transverse Momentum Broadening via Dihadron and Hadron-jet Angular Correlations in Relativistic Heavy-ion Collisions”, *Phys. Lett. B* **773** (2017) 672–676, arXiv:1607.01932 [hep-ph].
- [52] F. D’Eramo, K. Rajagopal, and Y. Yin, “Molière scattering in quark-gluon plasma: finding point-like scatterers in a liquid”, *JHEP* **01** (2019) 172, arXiv:1808.03250 [hep-ph].
- [53] ALICE Collaboration, K. Aamodt *et al.*, “The ALICE experiment at the CERN LHC”, *JINST* **3** (2008) S08002.
- [54] ALICE Collaboration, B. Abelev *et al.*, “Performance of the ALICE Experiment at the CERN LHC”, *Int. J. Mod. Phys. A* **29** (2014) 1430044, arXiv:1402.4476 [nucl-ex].
- [55] ALICE Collaboration, E. Abbas *et al.*, “Performance of the ALICE VZERO system”, *JINST* **8** (2013) P10016, arXiv:1306.3130 [nucl-ex].
- [56] ALICE Collaboration, S. Acharya *et al.*, “Measurement of charged jet cross section in pp collisions at $\sqrt{s} = 5.02$ TeV”, *Phys. Rev. D* **100** (2019) 092004, arXiv:1905.02536 [nucl-ex].
- [57] T. Sjöstrand, S. Mrenna, and P. Z. Skands, “A Brief Introduction to PYTHIA 8.1”, *Comput. Phys. Commun.* **178** (2008) 852–867, arXiv:hep-ph/0710.3820 [hep-ph].
- [58] P. Skands, S. Carrazza, and J. Rojo, “Tuning PYTHIA 8.1: the Monash 2013 Tune”, *Eur. Phys. J.*


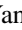

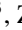









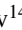
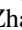

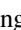
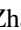







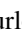
- C* **74** (2014) 3024, arXiv:1404.5630 [hep-ph].
- [59] R. Brun, F. Bruyant, M. Maire, A. C. McPherson, and P. Zancarini, *GEANT 3: user's guide Geant 3.10, Geant 3.11; rev. version*. CERN, Geneva, 1987. <https://cds.cern.ch/record/1119728>.
- [60] ALICE Collaboration, P. Cortese *et al.*, *ALICE forward detectors: FMD, T0 and V0: Technical Design Report*. 2004. <https://cds.cern.ch/record/781854>.
- [61] M. Cacciari, G. P. Salam, and G. Soyez, “FastJet User Manual”, *Eur. Phys. J. C* **72** (2012) 1896, arXiv:1111.6097 [hep-ph].
- [62] M. Cacciari and G. P. Salam, “Pileup subtraction using jet areas”, *Phys. Lett. B* **659** (2008) 119–126, arXiv:0707.1378 [hep-ph].
- [63] M. Cacciari, G. P. Salam, and G. Soyez, “The Catchment Area of Jets”, *JHEP* **04** (2008) 005, arXiv:0802.1188 [hep-ph].
- [64] ALICE Collaboration, S. Acharya *et al.*, “Multiplicity dependence of charged-particle jet production in pp collisions at $\sqrt{s} = 13$ TeV”, *Eur. Phys. J. C* **82** (2022) 514, arXiv:2202.01548 [nucl-ex].
- [65] D. de Florian, “Next-to-leading order QCD corrections to hadron+jet production in pp collisions at RHIC”, *Phys.Rev.* **D79** (2009) 114014, arXiv:0904.4402 [hep-ph].
- [66] ALICE Collaboration, S. Acharya *et al.*, “The ALICE definition of primary particles”, *ALICE-PUBLIC-2017-005* (2017) . <https://cds.cern.ch/record/2270008>.
- [67] ALICE Collaboration, B. Abelev *et al.*, “Measurement of charged jet suppression in Pb–Pb collisions at $\sqrt{s_{NN}} = 2.76$ TeV”, *JHEP* **03** (2014) 013, arXiv:1311.0633 [nucl-ex].
- [68] G. D’Agostini, “Improved iterative Bayesian unfolding”, arXiv:1010.0632 [physics.data-an].
- [69] T. Auye, “Unfolding algorithms and tests using RooUnfold”, *CERN-2011-006* (2011) 313–318.
- [70] S. Frixione, P. Nason, and C. Oleari, “Matching NLO QCD computations with Parton Shower simulations: the POWHEG method”, *JHEP* **0711** (2007) 070, arXiv:0709.2092 [hep-ph].
- [71] S. Alioli, K. Hamilton, P. Nason, C. Oleari, and R. Emanuele, “Jet pair production in POWHEG”, *JHEP* **04** (2011) 081, arXiv:1012.3380 [hep-ph].
- [72] P. Sun, C. P. Yuan, and F. Yuan, “Soft Gluon Resummations in Dijet Azimuthal Angular Correlations in Hadronic Collisions”, *Phys. Rev. Lett.* **113** (2014) 232001, arXiv:1405.1105 [hep-ph].
- [73] P. Sun, C. P. Yuan, and F. Yuan, “Transverse Momentum Resummation for Dijet Correlation in Hadronic Collisions”, *Phys. Rev. D* **92** (2015) 094007, arXiv:1506.06170 [hep-ph].

A The ALICE Collaboration

S. Acharya ¹²⁸, D. Adamová ⁸⁷, G. Aglieri Rinella ³³, M. Agnello ³⁰, N. Agrawal ⁵², Z. Ahammed ¹³⁶, S. Ahmad ¹⁶, S.U. Ahn ⁷², I. Ahuja ³⁸, A. Akhmedov ¹⁴², M. Al-Turany ⁹⁸, D. Aleksandrov ¹⁴², B. Alessandro ⁵⁷, H.M. Alfanda ⁶, R. Alfaro Molina ⁶⁸, B. Ali ¹⁶, A. Alici ²⁶, N. Alizadehvandchali ¹¹⁷, A. Alkin ³³, J. Alme ²¹, G. Alocco ⁵³, T. Alt ⁶⁵, A.R. Altamura ⁵¹, I. Altsybeev ⁹⁶, J.R. Alvarado ⁴⁵, M.N. Anaam ⁶, C. Andrei ⁴⁶, N. Andreou ¹¹⁶, A. Andronic ¹²⁷, V. Anguelov ⁹⁵, F. Antinori ⁵⁵, P. Antonioli ⁵², N. Apadula ⁷⁵, L. Aphecetche ¹⁰⁴, H. Appelshäuser ⁶⁵, C. Arata ⁷⁴, S. Arcelli ²⁶, M. Aresti ²³, R. Arnaldi ⁵⁷, J.G.M.C.A. Arneiro ¹¹¹, I.C. Arsene ²⁰, M. Arslandok ¹³⁹, A. Augustinus ³³, R. Averbeck ⁹⁸, M.D. Azmi ¹⁶, H. Baba ¹²⁵, A. Badalà ⁵⁴, J. Bae ¹⁰⁵, Y.W. Baek ⁴¹, X. Bai ¹²¹, R. Bailhache ⁶⁵, Y. Bailung ⁴⁹, A. Balbino ³⁰, A. Baldisseri ¹³¹, B. Balis ², D. Banerjee ⁴, Z. Banoo ⁹², R. Barbera ²⁷, F. Barile ³², L. Barioglio ⁹⁶, M. Barlou ⁷⁹, B. Barman ⁴², G.G. Barnaföldi ⁴⁷, L.S. Barnby ⁸⁶, V. Barret ¹²⁸, L. Barreto ¹¹¹, C. Bartels ¹²⁰, K. Barth ³³, E. Bartsch ⁶⁵, N. Bastid ¹²⁸, S. Basu ⁷⁶, G. Batigne ¹⁰⁴, D. Battistini ⁹⁶, B. Batyunya ¹⁴³, D. Bauri ⁴⁸, J.L. Bazo Alba ¹⁰², I.G. Bearden ⁸⁴, C. Beattie ¹³⁹, P. Becht ⁹⁸, D. Behera ⁴⁹, I. Belikov ¹³⁰, A.D.C. Bell Hechavarria ¹²⁷, F. Bellini ²⁶, R. Bellwied ¹¹⁷, S. Belokurova ¹⁴², Y.A.V. Beltran ⁴⁵, G. Bencedi ⁴⁷, S. Beole ²⁵, Y. Berdnikov ¹⁴², A. Berdnikova ⁹⁵, L. Bergmann ⁹⁵, M.G. Besoiu ⁶⁴, L. Betev ³³, P.P. Bhaduri ¹³⁶, A. Bhasin ⁹², M.A. Bhat ⁴, B. Bhattacharjee ⁴², L. Bianchi ²⁵, N. Bianchi ⁵⁰, J. Bielčík ³⁶, J. Bielčíková ⁸⁷, J. Biernat ¹⁰⁸, A.P. Bigot ¹³⁰, A. Bilandzic ⁹⁶, G. Biro ⁴⁷, S. Biswas ⁴, N. Bize ¹⁰⁴, J.T. Blair ¹⁰⁹, D. Blau ¹⁴², M.B. Blidaru ⁹⁸, N. Bluhme ³⁹, C. Blume ⁶⁵, G. Boca ^{22,56}, F. Bock ⁸⁸, T. Bodova ²¹, A. Bogdanov ¹⁴², S. Boi ²³, J. Bok ⁵⁹, L. Boldizsár ⁴⁷, M. Bombara ³⁸, P.M. Bond ³³, G. Bonomi ^{135,56}, H. Borel ¹³¹, A. Borissov ¹⁴², A.G. Borquez Carcamo ⁹⁵, H. Bossi ¹³⁹, E. Botta ²⁵, Y.E.M. Bouziani ⁶⁵, L. Bratrud ⁶⁵, P. Braun-Munzinger ⁹⁸, M. Bregant ¹¹¹, M. Broz ³⁶, G.E. Bruno ^{97,32}, M.D. Buckland ²⁴, D. Budnikov ¹⁴², H. Buesching ⁶⁵, S. Bufalino ³⁰, P. Buhler ¹⁰³, N. Burmasov ¹⁴², Z. Buthelezi ^{69,124}, A. Bylinkin ²¹, S.A. Bysiak ¹⁰⁸, M. Cai ⁶, H. Caines ¹³⁹, A. Caliva ²⁹, E. Calvo Villar ¹⁰², J.M.M. Camacho ¹¹⁰, P. Camerini ²⁴, F.D.M. Canedo ¹¹¹, S.L. Cantway ¹³⁹, M. Carabas ¹¹⁴, A.A. Carballo ³³, F. Carnesecchi ³³, R. Caron ¹²⁹, L.A.D. Carvalho ¹¹¹, J. Castillo Castellanos ¹³¹, F. Catalano ^{33,25}, C. Ceballos Sanchez ¹⁴³, I. Chakaberia ⁷⁵, P. Chakraborty ⁴⁸, S. Chandra ¹³⁶, S. Chapeland ³³, M. Chartier ¹²⁰, S. Chattopadhyay ¹³⁶, S. Chattopadhyay ¹⁰⁰, T. Cheng ^{98,6}, C. Cheshkov ¹²⁹, B. Cheynis ¹²⁹, V. Chibante Barroso ³³, D.D. Chinellato ¹¹², E.S. Chizzali ^{11,96}, J. Cho ⁵⁹, S. Cho ⁵⁹, P. Chochula ³³, D. Choudhury ⁴², P. Christakoglou ⁸⁵, C.H. Christensen ⁸⁴, P. Christiansen ⁷⁶, T. Chujo ¹²⁶, M. Ciaccio ³⁰, C. Cicalo ⁵³, F. Cindolo ⁵², M.R. Ciupek ⁹⁸, G. Clai ^{III,52}, F. Colamaria ⁵¹, J.S. Colburn ¹⁰¹, D. Colella ^{97,32}, M. Colocci ²⁶, M. Concas ³³, G. Conesa Balbastre ⁷⁴, Z. Conesa del Valle ¹³², G. Contin ²⁴, J.G. Contreras ³⁶, M.L. Coquet ¹³¹, P. Cortese ^{134,57}, M.R. Cosentino ¹¹³, F. Costa ³³, S. Costanza ^{22,56}, C. Cot ¹³², J. Crkovská ⁹⁵, P. Crochet ¹²⁸, R. Cruz-Torres ⁷⁵, P. Cui ⁶, A. Dainese ⁵⁵, M.C. Danisch ⁹⁵, A. Danu ⁶⁴, P. Das ⁸¹, P. Das ⁴, S. Das ⁴, A.R. Dash ¹²⁷, S. Dash ⁴⁸, A. De Caro ²⁹, G. de Cataldo ⁵¹, J. de Cuveland ³⁹, A. De Falco ²³, D. De Gruttola ²⁹, N. De Marco ⁵⁷, C. De Martin ²⁴, S. De Pasquale ²⁹, R. Deb ¹³⁵, R. Del Grande ⁹⁶, L. Dello Stritto ²⁹, W. Deng ⁶, P. Dhankher ¹⁹, D. Di Bari ³², A. Di Mauro ³³, B. Diab ¹³¹, R.A. Diaz ^{143,7}, T. Dietel ¹¹⁵, Y. Ding ⁶, J. Ditzel ⁶⁵, R. Divià ³³, D.U. Dixit ¹⁹, Ø. Djuvlsland ²¹, U. Dmitrieva ¹⁴², A. Dobrin ⁶⁴, B. Dönigus ⁶⁵, J.M. Dubinski ¹³⁷, A. Dubla ⁹⁸, S. Dudi ⁹¹, P. Dupieux ¹²⁸, M. Durkac ¹⁰⁷, N. Dzalaiova ¹³, T.M. Eder ¹²⁷, R.J. Ehlers ⁷⁵, F. Eisenhut ⁶⁵, R. Ejima ⁹³, D. Elia ⁵¹, B. Erazmus ¹⁰⁴, F. Ercolessi ²⁶, B. Espagnon ¹³², G. Eulisse ³³, D. Evans ¹⁰¹, S. Evdokimov ¹⁴², L. Fabbietti ⁹⁶, M. Faggin ²⁸, J. Faivre ⁷⁴, F. Fan ⁶, W. Fan ⁷⁵, A. Fantoni ⁵⁰, M. Fasel ⁸⁸, P. Fedichio ³⁰, A. Feliciello ⁵⁷, G. Feofilov ¹⁴², A. Fernández Téllez ⁴⁵, L. Ferrandi ¹¹¹, M.B. Ferrer ³³, A. Ferrero ¹³¹, C. Ferrero ^{IV,57}, A. Ferretti ²⁵, V.J.G. Feuillard ⁹⁵, V. Filova ³⁶, D. Finogeev ¹⁴², F.M. Fionda ⁵³, E. Flatland ³³, F. Flor ¹¹⁷, A.N. Flores ¹⁰⁹, S. Foertsch ⁶⁹, I. Fokin ⁹⁵, S. Fokin ¹⁴², E. Fragiaco ⁵⁸, E. Frajna ⁴⁷, U. Fuchs ³³, N. Funicello ²⁹, C. Furget ⁷⁴, A. Furs ¹⁴², T. Fusayasu ⁹⁹, J.J. Gaardhøje ⁸⁴, M. Gagliardi ²⁵, A.M. Gago ¹⁰², T. Gahlaut ⁴⁸, C.D. Galvan ¹¹⁰, D.R. Gangadharan ¹¹⁷, P. Ganoti ⁷⁹, C. Garabatos ⁹⁸, T. García Chávez ⁴⁵, E. García-Solis ⁹, C. Gargiulo ³³, P. Gasik ⁹⁸, A. Gautam ¹¹⁹, M.B. Gay Ducati ⁶⁷, M. Germain ¹⁰⁴, A. Ghimouz ¹²⁶, C. Ghosh ¹³⁶, M. Giacalone ⁵², G. Gioachin ³⁰, P. Giubellino ^{98,57}, P. Giubilato ²⁸, A.M.C. Glaenger ¹³¹, P. Gläsel ⁹⁵, E. Glimos ¹²³, D.J.Q. Goh ⁷⁷, V. Gonzalez ¹³⁸, M. Gorgon ², K. Goswami ⁴⁹, S. Gotovac ³⁴, V. Grabski ⁶⁸, L.K. Graczykowski ¹³⁷, E. Grecka ⁸⁷, A. Grelli ⁶⁰, C. Grigoras ³³, V. Grigoriev ¹⁴², S. Grigoryan ^{143,1}, F. Grosa ³³, J.F. Grosse-Oetringhaus ³³, R. Grosso ⁹⁸, D. Grund ³⁶, N.A. Grunwald ⁹⁵, G.G. Guardiano ¹¹², R. Guernane ⁷⁴, M. Guilbaud ¹⁰⁴, K. Gulbrandsen ⁸⁴, T. Gündem ⁶⁵, T. Gunji ¹²⁵,

W. Guo⁶, A. Gupta⁹², R. Gupta⁹², R. Gupta⁴⁹, K. Gwizdziel¹³⁷, L. Gyulai⁴⁷, C. Hadjidakis¹³², F.U. Haider⁹², S. Haidlova³⁶, H. Hamagaki⁷⁷, A. Hamdi⁷⁵, Y. Han¹⁴⁰, B.G. Hanley¹³⁸, R. Hannigan¹⁰⁹, J. Hansen⁷⁶, M.R. Haque¹³⁷, J.W. Harris¹³⁹, A. Harton⁹, H. Hassan¹¹⁸, D. Hatzifotiadou⁵², P. Hauer⁴³, L.B. Havener¹³⁹, S.T. Heckel⁹⁶, E. Hellbär⁹⁸, H. Helstrup³⁵, M. Hemmer⁶⁵, T. Herman³⁶, G. Herrera Corral⁸, F. Herrmann¹²⁷, S. Herrmann¹²⁹, K.F. Hetland³⁵, B. Heybeck⁶⁵, H. Hillemanns³³, B. Hippolyte¹³⁰, F.W. Hoffmann⁷¹, B. Hofman⁶⁰, G.H. Hong¹⁴⁰, M. Horst⁹⁶, A. Horzyk², Y. Hou⁶, P. Hristov³³, C. Hughes¹²³, P. Huhn⁶⁵, L.M. Huhta¹¹⁸, T.J. Humanic⁸⁹, A. Hutson¹¹⁷, D. Hutter³⁹, R. Ilkaev¹⁴², H. Ilyas¹⁴, M. Inaba¹²⁶, G.M. Innocenti³³, M. Ippolitov¹⁴², A. Isakov^{85,87}, T. Isidori¹¹⁹, M.S. Islam¹⁰⁰, M. Ivanov⁹⁸, M. Ivanov¹³, V. Ivanov¹⁴², K.E. Iversen⁷⁶, M. Jablonski², B. Jacak⁷⁵, N. Jacazio²⁶, P.M. Jacobs⁷⁵, S. Jadlovská¹⁰⁷, J. Jadlovsky¹⁰⁷, S. Jaelani⁸³, C. Jahnke¹¹¹, M.J. Jakubowska¹³⁷, M.A. Janik¹³⁷, T. Janson⁷¹, S. Ji¹⁷, S. Jia¹⁰, A.A.P. Jimenez⁶⁶, F. Jonas^{88,127}, D.M. Jones¹²⁰, J.M. Jowett^{33,98}, J. Jung⁶⁵, M. Jung⁶⁵, A. Junique³³, A. Jusko¹⁰¹, J. Kaewjai¹⁰⁶, P. Kalinak⁶¹, A.S. Kalteyer⁹⁸, A. Kalweit³³, V. Kaplin¹⁴², A. Karasu Uysal⁷³, D. Karatovic⁹⁰, O. Karavichev¹⁴², T. Karavicheva¹⁴², P. Karczmarczyk¹³⁷, E. Karpechev¹⁴², M.J. Karwowska^{33,137}, U. Keschull⁷¹, R. Keidel¹⁴¹, D.L.D. Keijdener⁶⁰, M. Keil³³, B. Ketzer⁴³, S.S. Khade⁴⁹, A.M. Khan¹²¹, S. Khan¹⁶, A. Khanzadeev¹⁴², Y. Kharlov¹⁴², A. Khatun¹¹⁹, A. Khuntia³⁶, B. Kileng³⁵, B. Kim¹⁰⁵, C. Kim¹⁷, D.J. Kim¹¹⁸, E.J. Kim⁷⁰, J. Kim¹⁴⁰, J.S. Kim⁴¹, J. Kim⁵⁹, J. Kim⁷⁰, M. Kim¹⁹, S. Kim¹⁸, T. Kim¹⁴⁰, K. Kimura⁹³, S. Kirsch⁶⁵, I. Kisel³⁹, S. Kiselev¹⁴², A. Kisiel¹³⁷, J.P. Kitowski², J.L. Klay⁵, J. Klein³³, S. Klein⁷⁵, C. Klein-Bösing¹²⁷, M. Kleiner⁶⁵, T. Klemenz⁹⁶, A. Kluge³³, A.G. Knospe¹¹⁷, C. Kobdaj¹⁰⁶, T. Kollegger⁹⁸, A. Kondratyev¹⁴³, N. Kondratyeva¹⁴², E. Kondratyuk¹⁴², J. König⁶⁵, S.A. Königstorfer⁹⁶, P.J. Konopka³³, G. Kornakov¹³⁷, M. Korwieser⁹⁶, S.D. Koryciak², A. Kotliarov^{87,36}, V. Kovalenko¹⁴², M. Kowalski¹⁰⁸, V. Kozuharov³⁷, I. Králik⁶¹, A. Kravčáková³⁸, L. Krcal^{33,39}, M. Krivda^{101,61}, F. Krizek⁸⁷, K. Krizkova Gajdosova³³, M. Kroesen⁹⁵, M. Krüger⁶⁵, D.M. Krupova³⁶, E. Kryshen¹⁴², V. Kučera⁵⁹, C. Kuhn¹³⁰, P.G. Kuijer⁸⁵, T. Kumaoka¹²⁶, D. Kumar¹³⁶, L. Kumar⁹¹, N. Kumar⁹¹, S. Kumar³², S. Kundu³³, P. Kurashvili⁸⁰, A. Kurepin¹⁴², A.B. Kurepin¹⁴², A. Kuryakin¹⁴², S. Kushpil⁸⁷, M.J. Kweon⁵⁹, Y. Kwon¹⁴⁰, S.L. La Pointe³⁹, P. La Rocca²⁷, A. Lakrathok¹⁰⁶, M. Lamanna³³, A.R. Landou^{74,116}, R. Langoy¹²², P. Larionov³³, E. Laudi³³, L. Lautner^{33,96}, R. Lavicka¹⁰³, R. Lea^{135,56}, H. Lee¹⁰⁵, I. Legrand⁴⁶, G. Le Gras¹²⁷, J. Lehrbach³⁹, T.M. Lelek², R.C. Lemmon⁸⁶, I. León Monzón¹¹⁰, M.M. Lesch⁹⁶, E.D. Lesser¹⁹, P. Lévai⁴⁷, X. Li¹⁰, J. Lien¹²², R. Lietava¹⁰¹, I. Likmeta¹¹⁷, B. Lim²⁵, S.H. Lim¹⁷, V. Lindenstruth³⁹, A. Lindner⁴⁶, C. Lippmann⁹⁸, D.H. Liu⁶, J. Liu¹²⁰, G.S.S. Liveraro¹¹², I.M. Lofnes²¹, C. Loizides⁸⁸, S. Lokos¹⁰⁸, J. Lömker⁶⁰, P. Loncar³⁴, X. Lopez¹²⁸, E. López Torres⁷, P. Lu^{98,121}, F.V. Lugo⁶⁸, J.R. Luhder¹²⁷, M. Lunardon²⁸, G. Luparello⁵⁸, Y.G. Ma⁴⁰, M. Mager³³, A. Maire¹³⁰, E.M. Majerz², M.V. Makariev³⁷, M. Malaev¹⁴², G. Malfattore²⁶, N.M. Malik⁹², Q.W. Malik²⁰, S.K. Malik⁹², L. Malinina^{I,VIII,143}, D. Mallick^{132,81}, N. Mallick⁴⁹, G. Mandaglio^{31,54}, S.K. Mandal⁸⁰, V. Manko¹⁴², F. Manso¹²⁸, V. Manzari⁵¹, Y. Mao⁶, R.W. Marcjan², G.V. Margagliotti²⁴, A. Margotti⁵², A. Marín⁹⁸, C. Markert¹⁰⁹, P. Martinengo³³, M.I. Martínez⁴⁵, G. Martínez García¹⁰⁴, M.P.P. Martins¹¹¹, S. Masciocchi⁹⁸, M. Masera²⁵, A. Masoni⁵³, L. Massacrier¹³², O. Massen⁶⁰, A. Mastroserio^{133,51}, O. Matonoha⁷⁶, S. Mattiazzo²⁸, A. Matyja¹⁰⁸, C. Mayer¹⁰⁸, A.L. Mazuecos³³, F. Mazzaschi²⁵, M. Mazzilli³³, J.E. Mdhuli¹²⁴, Y. Melikyan⁴⁴, A. Menchaca-Rocha⁶⁸, J.E.M. Mendez⁶⁶, E. Meninno¹⁰³, A.S. Menon¹¹⁷, M. Meres¹³, S. Mhlanga^{115,69}, Y. Miake¹²⁶, L. Micheletti³³, D.L. Mihaylov⁹⁶, K. Mikhaylov^{143,142}, A.N. Mishra⁴⁷, D. Miśkowiec⁹⁸, A. Modak⁴, B. Mohanty⁸¹, M. Mohisin Khan^{VI,16}, M.A. Molander⁴⁴, S. Monira¹³⁷, C. Mordasini¹¹⁸, D.A. Moreira De Godoy¹²⁷, I. Morozov¹⁴², A. Morsch³³, T. Mrnjavac³³, V. Muccifora⁵⁰, S. Muhuri¹³⁶, J.D. Mulligan⁷⁵, A. Mulliri²³, M.G. Munhoz¹¹¹, R.H. Munzer⁶⁵, H. Murakami¹²⁵, S. Murray¹¹⁵, L. Musa³³, J. Musinsky⁶¹, J.W. Myrcha¹³⁷, B. Naik¹²⁴, A.I. Nambrath¹⁹, B.K. Nandi⁴⁸, R. Nania⁵², E. Nappi⁵¹, A.F. Nassirpour¹⁸, A. Nath⁹⁵, C. Nattrass¹²³, M.N. Naydenov³⁷, A. Neagu²⁰, A. Negru¹¹⁴, L. Nellen⁶⁶, R. Nepeivoda⁷⁶, S. Nese²⁰, G. Neskovic³⁹, N. Nicassio⁵¹, B.S. Nielsen⁸⁴, E.G. Nielsen⁸⁴, S. Nikolaev¹⁴², S. Nikulin¹⁴², V. Nikulin¹⁴², F. Noferini⁵², S. Noh¹², P. Nomokonov¹⁴³, J. Norman¹²⁰, N. Novitzky⁸⁸, P. Nowakowski¹³⁷, A. Nyanin¹⁴², J. Nystrand²¹, M. Ogino⁷⁷, S. Oh¹⁸, A. Ohlson⁷⁶, V.A. Okorokov¹⁴², J. Oleniacz¹³⁷, A.C. Oliveira Da Silva¹²³, A. Onnerstad¹¹⁸, C. Oppedisano⁵⁷, A. Ortiz Velasquez⁶⁶, J. Otwinowski¹⁰⁸, M. Oya⁹³, K. Oyama⁷⁷, Y. Pachmayer⁹⁵, S. Padhan⁴⁸, D. Pagano^{135,56}, G. Paic⁶⁶, S. Paisano-Guzmán⁴⁵, A. Palasciano⁵¹,

S. Panebianco ¹³¹, H. Park ¹²⁶, H. Park ¹⁰⁵, J. Park ⁵⁹, J.E. Parkkila ³³, Y. Patley ⁴⁸, R.N. Patra ⁹²,
 B. Paul ²³, H. Pei ⁶, T. Peitzmann ⁶⁰, X. Peng ¹¹, M. Pennisi ²⁵, S. Perciballi ²⁵, D. Peresunko ¹⁴²,
 G.M. Perez ⁷, Y. Pestov ¹⁴², V. Petrov ¹⁴², M. Petrovici ⁴⁶, R.P. Pezzi ^{104,67}, S. Piano ⁵⁸, M. Pikna ¹³,
 P. Pillot ¹⁰⁴, O. Pinazza ^{52,33}, L. Pinsky ¹¹⁷, C. Pinto ⁹⁶, S. Pisano ⁵⁰, M. Płoskoń ⁷⁵, M. Planinic ⁹⁰,
 F. Pliquett ⁶⁵, M.G. Poghosyan ⁸⁸, B. Polichtchouk ¹⁴², S. Politano ³⁰, N. Poljak ⁹⁰, A. Pop ⁴⁶,
 S. Porteboeuf-Houssais ¹²⁸, V. Pozdniakov ¹⁴³, I.Y. Pozos ⁴⁵, K.K. Pradhan ⁴⁹, S.K. Prasad ⁴,
 S. Prasad ⁴⁹, R. Preghenella ⁵², F. Prino ⁵⁷, C.A. Pruneau ¹³⁸, I. Pshenichnov ¹⁴², M. Puccio ³³,
 S. Pucillo ²⁵, Z. Pugelova ¹⁰⁷, S. Qiu ⁸⁵, L. Quaglia ²⁵, S. Ragoni ¹⁵, A. Rai ¹³⁹,
 A. Rakotozafindrabe ¹³¹, L. Ramello ^{134,57}, F. Rami ¹³⁰, T.A. Rancien ⁷⁴, M. Rasa ²⁷, S.S. Räsänen ⁴⁴,
 R. Rath ⁵², M.P. Rauch ²¹, I. Ravasenga ⁸⁵, K.F. Read ^{88,123}, C. Reckziegel ¹¹³, A.R. Redelbach ³⁹,
 K. Redlich ^{VII,80}, C.A. Reetz ⁹⁸, H.D. Regules-Medel ⁴⁵, A. Rehman ²¹, F. Reidt ³³, H.A. Reme-Ness ³⁵,
 Z. Rescakova ³⁸, K. Reygers ⁹⁵, A. Riabov ¹⁴², V. Riabov ¹⁴², R. Ricci ²⁹, M. Richter ²⁰,
 A.A. Riedel ⁹⁶, W. Riegler ³³, A.G. Riffero ²⁵, C. Ristea ⁶⁴, M.V. Rodriguez ³³, M. Rodríguez
 Cahuantzi ⁴⁵, S.A. Rodríguez Ramírez ⁴⁵, K. Røed ²⁰, R. Rogalev ¹⁴², E. Rogochaya ¹⁴³,
 T.S. Rogoschinski ⁶⁵, D. Rohr ³³, D. Röhrich ²¹, P.F. Rojas ⁴⁵, S. Rojas Torres ³⁶, P.S. Rokita ¹³⁷,
 G. Romanenko ²⁶, F. Ronchetti ⁵⁰, A. Rosano ^{31,54}, E.D. Rosas ⁶⁶, K. Roslon ¹³⁷, A. Rossi ⁵⁵,
 A. Roy ⁴⁹, S. Roy ⁴⁸, N. Rubini ²⁶, D. Ruggiano ¹³⁷, R. Rui ²⁴, P.G. Russek ², R. Russo ⁸⁵,
 A. Rustamov ⁸², E. Ryabinkin ¹⁴², Y. Ryabov ¹⁴², A. Rybicki ¹⁰⁸, H. Rytönen ¹¹⁸, J. Ryu ¹⁷,
 W. Rzesza ¹³⁷, O.A.M. Saariimaki ⁴⁴, S. Sadhu ³², S. Sadovsky ¹⁴², J. Saetre ²¹, K. Šafařík ³⁶, P. Saha ⁴²,
 S.K. Saha ⁴, S. Saha ⁸¹, B. Sahoo ⁴⁸, B. Sahoo ⁴⁹, R. Sahoo ⁴⁹, S. Sahoo ⁶², D. Sahu ⁴⁹, P.K. Sahu ⁶²,
 J. Saini ¹³⁶, K. Sajdakova ³⁸, S. Sakai ¹²⁶, M.P. Salvan ⁹⁸, S. Sambyal ⁹², D. Samitz ¹⁰³, I. Sanna ^{33,96},
 T.B. Saramela ¹¹¹, P. Sarma ⁴², V. Sarritzu ²³, V.M. Sarti ⁹⁶, M.H.P. Sas ³³, S. Sawan ⁸¹,
 J. Schambach ⁸⁸, H.S. Scheid ⁶⁵, C. Schiaua ⁴⁶, R. Schicker ⁹⁵, F. Schlepfer ⁹⁵, A. Schmah ⁹⁸,
 C. Schmidt ⁹⁸, H.R. Schmidt ⁹⁴, M.O. Schmidt ³³, M. Schmidt ⁹⁴, N.V. Schmidt ⁸⁸, A.R. Schmier ¹²³,
 R. Schotter ¹³⁰, A. Schröter ³⁹, J. Schukraft ³³, K. Schweda ⁹⁸, G. Scioli ²⁶, E. Scomparin ⁵⁷,
 J.E. Seger ¹⁵, Y. Sekiguchi ¹²⁵, D. Sekihata ¹²⁵, M. Selina ⁸⁵, I. Selyuzhenkov ⁹⁸, S. Senyukov ¹³⁰,
 J.J. Seo ^{95,59}, D. Serebryakov ¹⁴², L. Šerkšnytė ⁹⁶, A. Sevcenco ⁶⁴, T.J. Shaba ⁶⁹, A. Shabetai ¹⁰⁴,
 R. Shahoyan ³³, A. Shangaraev ¹⁴², A. Sharma ⁹¹, B. Sharma ⁹², D. Sharma ⁴⁸, H. Sharma ^{55,108},
 M. Sharma ⁹², S. Sharma ⁷⁷, S. Sharma ⁹², U. Sharma ⁹², A. Shatat ¹³², O. Sheibani ¹¹⁷, K. Shigaki ⁹³,
 M. Shimomura ⁷⁸, J. Shin ¹², S. Shirinkin ¹⁴², Q. Shou ⁴⁰, Y. Sibirak ¹⁴², S. Siddhanta ⁵³,
 T. Siemiarczuk ⁸⁰, T.F. Silva ¹¹¹, D. Silvermyr ⁷⁶, T. Simantathammakul ¹⁰⁶, R. Simeonov ³⁷, B. Singh ⁹²,
 B. Singh ⁹⁶, K. Singh ⁴⁹, R. Singh ⁸¹, R. Singh ⁹², R. Singh ⁴⁹, S. Singh ¹⁶, V.K. Singh ¹³⁶,
 V. Singhal ¹³⁶, T. Sinha ¹⁰⁰, B. Sitar ¹³, M. Sitta ^{134,57}, T.B. Skaali ²⁰, G. Skorodumovs ⁹⁵,
 M. Slupecki ⁴⁴, N. Smirnov ¹³⁹, R.J.M. Snellings ⁶⁰, E.H. Solheim ²⁰, J. Song ¹⁷, C. Sonnabend ^{33,98},
 F. Soramel ²⁸, A.B. Soto-hernandez ⁸⁹, R. Spijkers ⁸⁵, I. Sputowska ¹⁰⁸, J. Staa ⁷⁶, J. Stachel ⁹⁵,
 I. Stan ⁶⁴, P.J. Steffanic ¹²³, S.F. Stiefelmaier ⁹⁵, D. Stocco ¹⁰⁴, I. Storehaug ²⁰, P. Stratmann ¹²⁷,
 S. Strazzi ²⁶, A. Sturniolo ^{31,54}, C.P. Stylianidis ⁸⁵, A.A.P. Suaide ¹¹¹, C. Suire ¹³², M. Sukhanov ¹⁴²,
 M. Suljic ³³, R. Sultanov ¹⁴², V. Sumberia ⁹², S. Sumowidagdo ⁸³, S. Swain ⁶², I. Szarka ¹³,
 M. Szymkowski ¹³⁷, S.F. Taghavi ⁹⁶, G. Taillepied ⁹⁸, J. Takahashi ¹¹², G.J. Tambave ⁸¹, S. Tang ⁶,
 Z. Tang ¹²¹, J.D. Tapia Takaki ¹¹⁹, N. Tapus ¹¹⁴, L.A. Tarasovicova ¹²⁷, M.G. Tazila ⁴⁶, G.F. Tassielli ³²,
 A. Tauro ³³, A. Tavira García ¹³², G. Tejeda Muñoz ⁴⁵, A. Telesca ³³, L. Terlizzi ²⁵, C. Terrevoli ¹¹⁷,
 S. Thakur ⁴, D. Thomas ¹⁰⁹, A. Tikhonov ¹⁴², N. Tiltmann ¹²⁷, A.R. Timmins ¹¹⁷, M. Tkacik ¹⁰⁷,
 T. Tkacik ¹⁰⁷, A. Toia ⁶⁵, R. Tokumoto ⁹³, K. Tomohiro ⁹³, N. Topilskaya ¹⁴², M. Toppi ⁵⁰, T. Tork ¹³²,
 V.V. Torres ¹⁰⁴, A.G. Torres Ramos ³², A. Trifiro ^{31,54}, A.S. Triolo ^{33,31,54}, S. Tripathy ⁵²,
 T. Tripathy ⁴⁸, S. Trogolo ³³, V. Trubnikov ³, W.H. Trzaska ¹¹⁸, T.P. Trzcinski ¹³⁷, A. Tumkin ¹⁴²,
 R. Turrisi ⁵⁵, T.S. Tveter ²⁰, K. Ullaland ²¹, B. Ulukutlu ⁹⁶, A. Uras ¹²⁹, G.L. Usai ²³, M. Vala ³⁸,
 N. Valle ²², L.V.R. van Doremalen ⁶⁰, M. van Leeuwen ⁸⁵, C.A. van Veen ⁹⁵, R.J.G. van Weelden ⁸⁵,
 P. Vande Vyvre ³³, D. Varga ⁴⁷, Z. Varga ⁴⁷, P. Vargas Torres ⁶⁶, M. Vasileiou ⁷⁹, A. Vasiliev ¹⁴²,
 O. Vázquez Doce ⁵⁰, O. Vazquez Rueda ¹¹⁷, V. Vechernin ¹⁴², E. Vercellin ²⁵, S. Vergara Limón ⁴⁵,
 R. Verma ⁴⁸, L. Vermunt ⁹⁸, R. Vértesi ⁴⁷, M. Verweij ⁶⁰, L. Vickovic ³⁴, Z. Vilakazi ¹²⁴, O. Villalobos
 Baillie ¹⁰¹, A. Villani ²⁴, A. Vinogradov ¹⁴², T. Virgili ²⁹, M.M.O. Virta ¹¹⁸, V. Vislavicius ⁷⁶,
 A. Vodopyanov ¹⁴³, B. Volkel ³³, M.A. Völkl ⁹⁵, K. Voloshin ¹⁴², S.A. Voloshin ¹³⁸, G. Volpe ³², B. von
 Haller ³³, I. Vorobyev ⁹⁶, N. Vozniuk ¹⁴², J. Vrláková ³⁸, J. Wan ⁴⁰, C. Wang ⁴⁰, D. Wang ⁴⁰, Y. Wang ⁴⁰,
 Y. Wang ⁶, A. Wegrzynek ³³, F.T. Weiglhofer ³⁹, S.C. Wenzel ³³, J.P. Wessels ¹²⁷, J. Wiechula ⁶⁵,
 J. Wikne ²⁰, G. Wilk ⁸⁰, J. Wilkinson ⁹⁸, G.A. Willems ¹²⁷, B. Windelband ⁹⁵, M. Winn ¹³¹,
 J.R. Wright ¹⁰⁹, W. Wu ⁴⁰, Y. Wu ¹²¹, R. Xu ⁶, A. Yadav ⁴³, A.K. Yadav ¹³⁶, S. Yalcin ⁷³,

Y. Yamaguchi ⁹³, S. Yang²¹, S. Yano ⁹³, Z. Yin ⁶, I.-K. Yoo ¹⁷, J.H. Yoon ⁵⁹, H. Yu¹², S. Yuan²¹, A. Yuncu ⁹⁵, V. Zaccolo ²⁴, C. Zampolli ³³, F. Zanone ⁹⁵, N. Zardoshti ³³, A. Zarochentsev ¹⁴², P. Závada ⁶³, N. Zaviyalov¹⁴², M. Zhalov ¹⁴², B. Zhang ⁶, C. Zhang ¹³¹, L. Zhang ⁴⁰, M. Zhang⁶, S. Zhang ⁴⁰, X. Zhang ⁶, Y. Zhang¹²¹, Z. Zhang ⁶, M. Zhao ¹⁰, V. Zhrebchevskii ¹⁴², Y. Zhi¹⁰, D. Zhou ⁶, Y. Zhou ⁸⁴, J. Zhu ^{55,6}, Y. Zhu⁶, S.C. Zugravel ⁵⁷, N. Zurlo ^{135,56}

Affiliation Notes

^I Deceased

^{II} Also at: Max-Planck-Institut für Physik, Munich, Germany

^{III} Also at: Italian National Agency for New Technologies, Energy and Sustainable Economic Development (ENEA), Bologna, Italy

^{IV} Also at: Dipartimento DET del Politecnico di Torino, Turin, Italy

^V Also at: Yildiz Technical University, Istanbul, Türkiye

^{VI} Also at: Department of Applied Physics, Aligarh Muslim University, Aligarh, India

^{VII} Also at: Institute of Theoretical Physics, University of Wrocław, Poland

^{VIII} Also at: An institution covered by a cooperation agreement with CERN

Collaboration Institutes

¹ A.I. Alikhanyan National Science Laboratory (Yerevan Physics Institute) Foundation, Yerevan, Armenia

² AGH University of Krakow, Cracow, Poland

³ Bogolyubov Institute for Theoretical Physics, National Academy of Sciences of Ukraine, Kiev, Ukraine

⁴ Bose Institute, Department of Physics and Centre for Astroparticle Physics and Space Science (CAPSS), Kolkata, India

⁵ California Polytechnic State University, San Luis Obispo, California, United States

⁶ Central China Normal University, Wuhan, China

⁷ Centro de Aplicaciones Tecnológicas y Desarrollo Nuclear (CEADEN), Havana, Cuba

⁸ Centro de Investigación y de Estudios Avanzados (CINVESTAV), Mexico City and Mérida, Mexico

⁹ Chicago State University, Chicago, Illinois, United States

¹⁰ China Institute of Atomic Energy, Beijing, China

¹¹ China University of Geosciences, Wuhan, China

¹² Chungbuk National University, Cheongju, Republic of Korea

¹³ Comenius University Bratislava, Faculty of Mathematics, Physics and Informatics, Bratislava, Slovak Republic

¹⁴ COMSATS University Islamabad, Islamabad, Pakistan

¹⁵ Creighton University, Omaha, Nebraska, United States

¹⁶ Department of Physics, Aligarh Muslim University, Aligarh, India

¹⁷ Department of Physics, Pusan National University, Pusan, Republic of Korea

¹⁸ Department of Physics, Sejong University, Seoul, Republic of Korea

¹⁹ Department of Physics, University of California, Berkeley, California, United States

²⁰ Department of Physics, University of Oslo, Oslo, Norway

²¹ Department of Physics and Technology, University of Bergen, Bergen, Norway

²² Dipartimento di Fisica, Università di Pavia, Pavia, Italy

²³ Dipartimento di Fisica dell'Università and Sezione INFN, Cagliari, Italy

²⁴ Dipartimento di Fisica dell'Università and Sezione INFN, Trieste, Italy

²⁵ Dipartimento di Fisica dell'Università and Sezione INFN, Turin, Italy

²⁶ Dipartimento di Fisica e Astronomia dell'Università and Sezione INFN, Bologna, Italy

²⁷ Dipartimento di Fisica e Astronomia dell'Università and Sezione INFN, Catania, Italy

²⁸ Dipartimento di Fisica e Astronomia dell'Università and Sezione INFN, Padova, Italy

²⁹ Dipartimento di Fisica 'E.R. Caianiello' dell'Università and Gruppo Collegato INFN, Salerno, Italy

³⁰ Dipartimento DISAT del Politecnico and Sezione INFN, Turin, Italy

³¹ Dipartimento di Scienze MIIFT, Università di Messina, Messina, Italy

³² Dipartimento Interateneo di Fisica 'M. Merlin' and Sezione INFN, Bari, Italy

³³ European Organization for Nuclear Research (CERN), Geneva, Switzerland

³⁴ Faculty of Electrical Engineering, Mechanical Engineering and Naval Architecture, University of Split, Split, Croatia

- ³⁵ Faculty of Engineering and Science, Western Norway University of Applied Sciences, Bergen, Norway
- ³⁶ Faculty of Nuclear Sciences and Physical Engineering, Czech Technical University in Prague, Prague, Czech Republic
- ³⁷ Faculty of Physics, Sofia University, Sofia, Bulgaria
- ³⁸ Faculty of Science, P.J. Šafárik University, Košice, Slovak Republic
- ³⁹ Frankfurt Institute for Advanced Studies, Johann Wolfgang Goethe-Universität Frankfurt, Frankfurt, Germany
- ⁴⁰ Fudan University, Shanghai, China
- ⁴¹ Gangneung-Wonju National University, Gangneung, Republic of Korea
- ⁴² Gauhati University, Department of Physics, Guwahati, India
- ⁴³ Helmholtz-Institut für Strahlen- und Kernphysik, Rheinische Friedrich-Wilhelms-Universität Bonn, Bonn, Germany
- ⁴⁴ Helsinki Institute of Physics (HIP), Helsinki, Finland
- ⁴⁵ High Energy Physics Group, Universidad Autónoma de Puebla, Puebla, Mexico
- ⁴⁶ Horia Hulubei National Institute of Physics and Nuclear Engineering, Bucharest, Romania
- ⁴⁷ HUN-REN Wigner Research Centre for Physics, Budapest, Hungary
- ⁴⁸ Indian Institute of Technology Bombay (IIT), Mumbai, India
- ⁴⁹ Indian Institute of Technology Indore, Indore, India
- ⁵⁰ INFN, Laboratori Nazionali di Frascati, Frascati, Italy
- ⁵¹ INFN, Sezione di Bari, Bari, Italy
- ⁵² INFN, Sezione di Bologna, Bologna, Italy
- ⁵³ INFN, Sezione di Cagliari, Cagliari, Italy
- ⁵⁴ INFN, Sezione di Catania, Catania, Italy
- ⁵⁵ INFN, Sezione di Padova, Padova, Italy
- ⁵⁶ INFN, Sezione di Pavia, Pavia, Italy
- ⁵⁷ INFN, Sezione di Torino, Turin, Italy
- ⁵⁸ INFN, Sezione di Trieste, Trieste, Italy
- ⁵⁹ Inha University, Incheon, Republic of Korea
- ⁶⁰ Institute for Gravitational and Subatomic Physics (GRASP), Utrecht University/Nikhef, Utrecht, Netherlands
- ⁶¹ Institute of Experimental Physics, Slovak Academy of Sciences, Košice, Slovak Republic
- ⁶² Institute of Physics, Homi Bhabha National Institute, Bhubaneswar, India
- ⁶³ Institute of Physics of the Czech Academy of Sciences, Prague, Czech Republic
- ⁶⁴ Institute of Space Science (ISS), Bucharest, Romania
- ⁶⁵ Institut für Kernphysik, Johann Wolfgang Goethe-Universität Frankfurt, Frankfurt, Germany
- ⁶⁶ Instituto de Ciencias Nucleares, Universidad Nacional Autónoma de México, Mexico City, Mexico
- ⁶⁷ Instituto de Física, Universidade Federal do Rio Grande do Sul (UFRGS), Porto Alegre, Brazil
- ⁶⁸ Instituto de Física, Universidad Nacional Autónoma de México, Mexico City, Mexico
- ⁶⁹ iThemba LABS, National Research Foundation, Somerset West, South Africa
- ⁷⁰ Jeonbuk National University, Jeonju, Republic of Korea
- ⁷¹ Johann-Wolfgang-Goethe Universität Frankfurt Institut für Informatik, Fachbereich Informatik und Mathematik, Frankfurt, Germany
- ⁷² Korea Institute of Science and Technology Information, Daejeon, Republic of Korea
- ⁷³ KTO Karatay University, Konya, Turkey
- ⁷⁴ Laboratoire de Physique Subatomique et de Cosmologie, Université Grenoble-Alpes, CNRS-IN2P3, Grenoble, France
- ⁷⁵ Lawrence Berkeley National Laboratory, Berkeley, California, United States
- ⁷⁶ Lund University Department of Physics, Division of Particle Physics, Lund, Sweden
- ⁷⁷ Nagasaki Institute of Applied Science, Nagasaki, Japan
- ⁷⁸ Nara Women's University (NWU), Nara, Japan
- ⁷⁹ National and Kapodistrian University of Athens, School of Science, Department of Physics, Athens, Greece
- ⁸⁰ National Centre for Nuclear Research, Warsaw, Poland
- ⁸¹ National Institute of Science Education and Research, Homi Bhabha National Institute, Jatni, India
- ⁸² National Nuclear Research Center, Baku, Azerbaijan
- ⁸³ National Research and Innovation Agency - BRIN, Jakarta, Indonesia
- ⁸⁴ Niels Bohr Institute, University of Copenhagen, Copenhagen, Denmark
- ⁸⁵ Nikhef, National institute for subatomic physics, Amsterdam, Netherlands
- ⁸⁶ Nuclear Physics Group, STFC Daresbury Laboratory, Daresbury, United Kingdom

- 87 Nuclear Physics Institute of the Czech Academy of Sciences, Husinec-Řež, Czech Republic
- 88 Oak Ridge National Laboratory, Oak Ridge, Tennessee, United States
- 89 Ohio State University, Columbus, Ohio, United States
- 90 Physics department, Faculty of science, University of Zagreb, Zagreb, Croatia
- 91 Physics Department, Panjab University, Chandigarh, India
- 92 Physics Department, University of Jammu, Jammu, India
- 93 Physics Program and International Institute for Sustainability with Knotted Chiral Meta Matter (SKCM2), Hiroshima University, Hiroshima, Japan
- 94 Physikalisches Institut, Eberhard-Karls-Universität Tübingen, Tübingen, Germany
- 95 Physikalisches Institut, Ruprecht-Karls-Universität Heidelberg, Heidelberg, Germany
- 96 Physik Department, Technische Universität München, Munich, Germany
- 97 Politecnico di Bari and Sezione INFN, Bari, Italy
- 98 Research Division and ExtreMe Matter Institute EMMI, GSI Helmholtzzentrum für Schwerionenforschung GmbH, Darmstadt, Germany
- 99 Saga University, Saga, Japan
- 100 Saha Institute of Nuclear Physics, Homi Bhabha National Institute, Kolkata, India
- 101 School of Physics and Astronomy, University of Birmingham, Birmingham, United Kingdom
- 102 Sección Física, Departamento de Ciencias, Pontificia Universidad Católica del Perú, Lima, Peru
- 103 Stefan Meyer Institut für Subatomare Physik (SMI), Vienna, Austria
- 104 SUBATECH, IMT Atlantique, Nantes Université, CNRS-IN2P3, Nantes, France
- 105 Sungkyunkwan University, Suwon City, Republic of Korea
- 106 Suranaree University of Technology, Nakhon Ratchasima, Thailand
- 107 Technical University of Košice, Košice, Slovak Republic
- 108 The Henryk Niewodniczanski Institute of Nuclear Physics, Polish Academy of Sciences, Cracow, Poland
- 109 The University of Texas at Austin, Austin, Texas, United States
- 110 Universidad Autónoma de Sinaloa, Culiacán, Mexico
- 111 Universidade de São Paulo (USP), São Paulo, Brazil
- 112 Universidade Estadual de Campinas (UNICAMP), Campinas, Brazil
- 113 Universidade Federal do ABC, Santo Andre, Brazil
- 114 Universitatea Nationala de Stiinta si Tehnologie Politehnica Bucuresti, Bucharest, Romania
- 115 University of Cape Town, Cape Town, South Africa
- 116 University of Derby, Derby, United Kingdom
- 117 University of Houston, Houston, Texas, United States
- 118 University of Jyväskylä, Jyväskylä, Finland
- 119 University of Kansas, Lawrence, Kansas, United States
- 120 University of Liverpool, Liverpool, United Kingdom
- 121 University of Science and Technology of China, Hefei, China
- 122 University of South-Eastern Norway, Kongsberg, Norway
- 123 University of Tennessee, Knoxville, Tennessee, United States
- 124 University of the Witwatersrand, Johannesburg, South Africa
- 125 University of Tokyo, Tokyo, Japan
- 126 University of Tsukuba, Tsukuba, Japan
- 127 Universität Münster, Institut für Kernphysik, Münster, Germany
- 128 Université Clermont Auvergne, CNRS/IN2P3, LPC, Clermont-Ferrand, France
- 129 Université de Lyon, CNRS/IN2P3, Institut de Physique des 2 Infinis de Lyon, Lyon, France
- 130 Université de Strasbourg, CNRS, IPHC UMR 7178, F-67000 Strasbourg, France, Strasbourg, France
- 131 Université Paris-Saclay, Centre d'Etudes de Saclay (CEA), IRFU, Département de Physique Nucléaire (DPhN), Saclay, France
- 132 Université Paris-Saclay, CNRS/IN2P3, IJCLab, Orsay, France
- 133 Università degli Studi di Foggia, Foggia, Italy
- 134 Università del Piemonte Orientale, Vercelli, Italy
- 135 Università di Brescia, Brescia, Italy
- 136 Variable Energy Cyclotron Centre, Homi Bhabha National Institute, Kolkata, India
- 137 Warsaw University of Technology, Warsaw, Poland
- 138 Wayne State University, Detroit, Michigan, United States
- 139 Yale University, New Haven, Connecticut, United States

¹⁴⁰ Yonsei University, Seoul, Republic of Korea

¹⁴¹ Zentrum für Technologie und Transfer (ZTT), Worms, Germany

¹⁴² Affiliated with an institute covered by a cooperation agreement with CERN

¹⁴³ Affiliated with an international laboratory covered by a cooperation agreement with CERN.